International Journal of Solids and Structures 47 (2010) 3377–3388

Contents lists available at ScienceDirect

International Journal of Solids and Structures

journal homepage: www.elsevier.com/locate/ijsolstr

Low-frequency dispersion of fundamental waves in anisotropic piezoelectric plates

A.L. Shuvalov [a,*], E. Le Clezio [b]

[a] Laboratoire de Mécanique Physique, Université de Bordeaux, CNRS, UMR 5469, Talence 33405, France
[b] Laboratoire Imagerie et Cerveau, Université François Rabelais de Tours, CNRS, FR 3110, Blois 41034, France

ARTICLE INFO

Article history:
Received 1 February 2010
Received in revised form 15 July 2010
Available online 22 August 2010

Keywords:
Piezoelectric plate
Low-frequency dispersion
Anisotropic
Functionally graded

ABSTRACT

Low-frequency onset of the fundamental branches in piezoplates is studied with a view to identify the impact of piezoelectric coupling. General analytical expressions for the zero- and leading-order terms of the velocity versus wavenumber expansion in an anisotropic homogeneous piezoplate are obtained. On this ground, it is shown what types of anisotropy and electric boundary conditions enable the onset parameters of fundamental branches to be piezoactive. Particular attention is given to the linear dispersion at the origin of two upper fundamental branches. This property is entirely caused by the piezoeffect, being ruled out for elastic plates. An invariant hierarchy is established between the zero-order velocities of the fundamental waves under different electric boundary conditions in homogeneous and functionally graded plates. It is shown that some of these velocities in a metallized plate become piezoactive specifically if the piezoplate is functionally graded.

1. Introduction

Analytical insight into the low-frequency long-wave dispersion in a traction-free plate is of interest from both applied and theoretical viewpoints. This spectral range is an output of a number of experimental techniques aimed at the non-destructive evaluation of plate material. Also the low-frequency dispersion coefficients are essential ingredients for various asymptotic and engineering plate theories. Much work continues to be done on this subject for piezoelectric plates (see Johansson and Niklasson, 2003; Cheng and Reddy, 2003; Krommer, 2003; Wang and Rokhlin, 2004; Joshi et al., 2006; Mauritsson et al., 2008; Kuznetsova et al., 2008; Mauritsson, 2009). However, there remain certain unexplored aspects, particularly those related to anisotropy. They have a direct practical implication for piezomaterial characterization, where one of the primary targets is the strength of piezoelectric coupling. It can be inferred from the low-frequency experimental data if the involved modes are piezoactive for the given plate geometry. This depends on the anisotropy. Additional diversity is brought about by the possibility to change the electric boundary conditions (EBC) through metallizing the plate faces. Knowing explicit expressions for low-frequency dispersion is therefore helpful for a judicious choice of the plate orientation and of the type of EBC for measuring the desirable piezoelectric coefficient. It is also interesting to establish the invariant inequalities that compare the onset of the fundamental branches in a given plate under different types of EBC.

Another motivation for the present study is to analyze the new features of the low-frequency dispersion that are entirely caused by the piezoelectric effect. This concerns the unusual, linear onset of the SH_0 and/or S_0 branches and in particular an upgoing slope of the S_0 branch, which have been observed numerically and experimentally (Yang and Chimenti, 1995; Yang and Huang, 2003). Both these features, the linear onset of these branches of itself and the upward trend of S_0, are fundamentally ruled out in a purely elastic plate of any anisotropy (Shuvalov, 2004; Shuvalov, 2006).

The paper is organized as follows. Section 2 outlines the background, whose technicalities are further detailed in the Appendix. Section 3 describes the low-frequency (long-wave) onset of fundamental branches in a homogeneous piezoelectric plate. In Section 3.1, the effect of piezoelectricity on the initial slope of the flexural branch $v_1(k)$ is discussed, and Mindlin's type approximation of the full extent of this branch is demonstrated. Section 3.2 deals with the two upper fundamental velocity branches $v_{2,3}(k)$ (termed SH_0 and S_0 if the plate is cut along a symmetry plane). Particular attention is given to their linear dispersion that does not exist in purely elastic plates. A detailed analysis and examples are provided in this Section for the azimuthal dependence of the long-wave dispersion in piezoelectric plates of typical orientations. Section 4 is concerned with a functionally graded piezoelectric plate, for which the slope of the flexural branch and the zero-frequency limiting velocity of two other fundamental waves are derived and analyzed.

* Corresponding author. Tel.: +33 5 40003137; fax: +33 5 40006964.
E-mail address: a.shuvalov@lmp.u-bordeaux1.fr (A.L. Shuvalov).

0020-7683/$ - see front matter © 2010 Elsevier Ltd. All rights reserved.
doi:10.1016/j.ijsolstr.2010.07.018

2. Background

2.1. Governing equations

Consider an infinite anisotropic piezoelectric plate and denote the lateral and transverse coordinates by $x = \mathbf{m}\cdot\mathbf{r}$ and $y = \mathbf{n}\cdot\mathbf{r}$, where $\mathbf{m}$ and $\mathbf{n}$ are unit vectors parallel and orthogonal to the plate faces, respectively (Fig. 1). We are concerned with plane harmonic acoustic waves travelling along $\mathbf{m}$ with the amplitude depending on y and with the phase factor $\exp[ik(x-vt)]$, in which k is wave number, $v=\omega/k$ phase velocity, and ω angular frequency. For a given plate with a fixed normal $\mathbf{n}$, the propagation direction $\mathbf{m}$ is defined through its azimuth angle θ.

The state-vector formalism of piezoacoustics (Lothe and Barnett, 1976; Lothe and Barnett, 1977) enables writing the governing equations in the suitable form

$$\mathrm{i}k\mathbf{N}\boldsymbol{\eta}(y) = \frac{\mathrm{d}\boldsymbol{\eta}(y)}{\mathrm{d}y} \tag{1}$$

with

$$\mathbf{N} = \begin{pmatrix} \mathbf{N}_1 & \mathbf{N}_2 \\ \mathbf{N}_3 - \rho v^2 \mathrm{diag}(\mathbf{I},0) & \mathbf{N}_1^{\mathrm{T}} \end{pmatrix},$$
$$\boldsymbol{\eta}(y) = \left(\mathbf{A}(y),\quad \phi(y),\quad \mathrm{i}k^{-1}\mathbf{F}(y),\quad \mathrm{i}k^{-1}D_y(y)\right)^{\mathrm{T}}, \tag{2}$$

where $^{\mathrm{T}}$ means transposition and $\mathbf{I}$ is the 3×3 identity matrix. The 8×8 system matrix $\mathbf{N}$ contains the density ρ of the plate material and its elastic, piezoelectric and dielectric coefficients c_{ijkl}, e_{ijk}, ε_{ij}, which are contracted with components of $\mathbf{m}$ and $\mathbf{n}$. The 8-component state vector $\boldsymbol{\eta}(y)$ consists of the amplitudes $\mathbf{A}$ and $\mathbf{F}(=\mathbf{n}\boldsymbol{\sigma})$ of the elastic displacement and traction, and of the amplitudes ϕ and D_y of electric potential and (normal) displacement taken, for instance, as the 4th and 8th components (the Φ-representation of Lothe and Barnett, 1976; Lothe and Barnett, 1977).

Following Ting (1996), it is convenient to further partition 4×4 blocks of $\mathbf{N}$ to the form

$$\mathbf{N}_1 = \begin{pmatrix} \hat{\mathbf{n}}_1 & \mathbf{a}_1 \\ \mathbf{a}_1^{\mathrm{T}} & b_1 \end{pmatrix},\quad \mathbf{N}_2 = \begin{pmatrix} \hat{\mathbf{n}}_2 & \mathbf{a}_2 \\ \mathbf{a}_2^{\mathrm{T}} & b_2 \end{pmatrix} = \mathbf{N}_2^{\mathrm{T}},\quad \mathbf{N}_3 = \begin{pmatrix} \hat{\mathbf{n}}_3 & \mathbf{a}_3 \\ \mathbf{a}_3^{\mathrm{T}} & b_3 \end{pmatrix} = \mathbf{N}_3^{\mathrm{T}}, \tag{3}$$

where the 3×3 matrices $\hat{\mathbf{n}}$, 3-component vectors $\mathbf{a}$, and scalars b are defined as follows:

$$\hat{\mathbf{n}}_1 = \mathbf{N}_1^{(\mathrm{els})} + \frac{1}{b_2}\mathbf{a}_2\otimes\mathbf{a}_1',\quad \hat{\mathbf{n}}_2 = \mathbf{N}_2^{(\mathrm{els})} + \frac{1}{b_2}\mathbf{a}_2\otimes\mathbf{a}_2,\quad \hat{\mathbf{n}}_3 = \mathbf{N}_3^{(\mathrm{els})} + \frac{1}{b_2}\mathbf{a}_1'\otimes\mathbf{a}_1';$$
$$\mathbf{a}_1 = \mathbf{N}_2^{(\mathrm{els})}(\mathbf{e}_{\mathbf{mn}} + b_1\mathbf{e}_{\mathbf{nn}}),\quad \mathbf{a}_1' = b_2\left(\mathbf{N}_1^{(\mathrm{els})\mathrm{T}}\mathbf{e}_{\mathbf{nn}} + \mathbf{e}_{\mathbf{nm}}\right),\quad \mathbf{a}_2 = b_2\mathbf{N}_2^{(\mathrm{els})}\mathbf{e}_{\mathbf{nn}},$$
$$\mathbf{a}_3 = \mathbf{N}_1^{(\mathrm{els})\mathrm{T}}(\mathbf{e}_{\mathbf{mn}} + b_1\mathbf{e}_{\mathbf{nn}}) + \mathbf{e}_{\mathbf{mm}} + b_1\mathbf{e}_{\mathbf{nm}};\quad b_1 = b_2\left(-\varepsilon_{\mathbf{nm}} + \mathbf{e}_{\mathbf{mn}}\cdot\mathbf{N}_2^{(\mathrm{els})}\mathbf{e}_{\mathbf{nn}}\right),$$
$$b_2 = \left(\varepsilon_{\mathbf{nn}} - \mathbf{e}_{\mathbf{nn}}\cdot\mathbf{N}_2^{(\mathrm{els})}\mathbf{e}_{\mathbf{nn}}\right)^{-1},\quad b_3 = \frac{b_1^2}{b_2} - \varepsilon_{\mathbf{mm}} + \mathbf{e}_{\mathbf{mn}}\cdot\mathbf{N}_2^{(\mathrm{els})}\mathbf{e}_{\mathbf{mn}}, \tag{4}$$

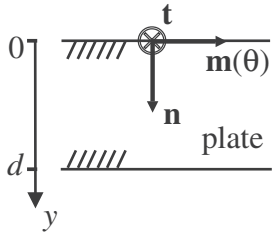

Fig. 1. Geometry of the problem.

$\otimes$ and $\cdot$ denote the outer (dyadic) and inner (scalar) products, $\mathbf{N}^{(\mathrm{els})}$ is the 6×6 Stroh matrix of elasticity, and $\mathbf{e}_{\mathbf{pq}}$, $\varepsilon_{\mathbf{pq}}$ denote the auxiliary 'piezoelectric vectors' and 'dielectric scalars' depending on $\mathbf{n}$ and $\mathbf{m}$:

$$\mathbf{N}^{(\mathrm{els})} = \begin{pmatrix} \mathbf{N}_1^{(\mathrm{els})} & \mathbf{N}_2^{(\mathrm{els})} \\ \mathbf{N}_3^{(\mathrm{els})} & \mathbf{N}_1^{(\mathrm{els})\mathrm{T}} \end{pmatrix},\quad \begin{matrix} \mathbf{N}_1^{(\mathrm{els})} = -\mathbf{c}_{\mathbf{nn}}^{-1}\mathbf{c}_{\mathbf{nm}},\quad \mathbf{N}_2^{(\mathrm{els})} = -\mathbf{c}_{\mathbf{nn}}^{-1}, \\ \mathbf{N}_3^{(\mathrm{els})} = \mathbf{c}_{\mathbf{mm}} - \mathbf{c}_{\mathbf{mn}}\mathbf{c}_{\mathbf{nn}}^{-1}\mathbf{c}_{\mathbf{nm}}, \end{matrix};$$
$$(\mathbf{c}_{\mathbf{pq}})_{jk} = p_i c_{ijkl} q_k;\quad (\mathbf{e}_{\mathbf{pq}})_j = p_i e_{ijk} q_k;\quad \varepsilon_{\mathbf{pq}} = p_i\varepsilon_{ij}q_j \text{ with } \mathbf{p},\mathbf{q} = \mathbf{m} \text{ or } \mathbf{n}. \tag{5}$$

In the case of pure elasticity ($e_{ijk}=0$), all vectors $\mathbf{e}_{\mathbf{pq}}$ and hence $\mathbf{a}$ vanish, and so the 3×3 blocks $\hat{\mathbf{n}}$ become 'purely elastic', i.e. $\hat{\mathbf{n}}_i = \mathbf{N}_i^{(\mathrm{els})}$, $i=1,2,3$. By (4),

$$\hat{\mathbf{n}}_3\mathbf{n} = \mathbf{N}_3^{(\mathrm{els})}\mathbf{n} = \mathbf{0},\ \hat{\mathbf{n}}_1\mathbf{n} = \mathbf{N}_1^{(\mathrm{els})}\mathbf{n} = -\mathbf{m},\ \mathbf{a}_1'\cdot\mathbf{n} = \mathbf{a}_3\cdot\mathbf{n} = 0;$$
$$b_2 > 0,\quad b_3 < 0. \tag{6}$$

Symmetric matrices $\mathbf{N}_2^{(\mathrm{els})}$ and $\hat{\mathbf{n}}_2$ are negative definite, and symmetric $\mathbf{N}_3^{(\mathrm{els})}$ and $\hat{\mathbf{n}}_3$ are positive semi-definite with a common null vector $\mathbf{n}$. Denote their remaining (apart from $\mathbf{n}$) eigen-pairs by

$$\hat{\mathbf{n}}_3\mathbf{f}_\alpha = \eta_\alpha\mathbf{f}_\alpha,\quad \mathbf{N}_3^{(\mathrm{els})}\mathbf{f}_\alpha^{(\mathrm{els})} = \eta_\alpha^{(\mathrm{els})}\mathbf{f}_\alpha^{(\mathrm{els})},\quad \alpha = 2,3, \tag{7}$$

where each set of eigenvectors is orthogonal ($\mathbf{f}_\alpha\cdot\mathbf{f}_\beta = \delta_{\alpha\beta}$, $\mathbf{f}_\alpha\cdot\mathbf{n}=0$ and $\mathbf{f}_\alpha^{(\mathrm{els})}\cdot\mathbf{f}_\beta^{(\mathrm{els})} = \delta_{\alpha\beta}$, $\mathbf{f}_\alpha^{(\mathrm{els})}\cdot\mathbf{n} = 0$) and the eigenvalues, numbered in the increasing order, satisfy the inequality

$$\eta_3 \geqslant \eta_3^{(\mathrm{els})} \geqslant \eta_2 \geqslant \eta_2^{(\mathrm{els})} > 0. \tag{8}$$

The eigenspectra of $\mathbf{N}_3^{(\mathrm{els})}$ and $\hat{\mathbf{n}}_3$ play an essential role in the low-frequency long-wave asymptotics, see Section 3.

2.2. Propagator matrix and dispersion equation

According to (1), the state vectors at the opposite faces $y=0$ and $y=d$ of either homogeneous or vertically inhomogeneous plate of thickness d satisfy the relation

$$\boldsymbol{\eta}(d) = \mathbf{M}(d,0)\boldsymbol{\eta}(0), \tag{9}$$

where $\mathbf{M}(d,0)$ is the propagator matrix defined in the homogeneous or inhomogeneous case as, respectively, a matrix exponential or a Peano series:

$$\mathbf{M}(d,0) = \begin{cases} \exp(\mathrm{i}kd\mathbf{N}), \\ \mathbf{I} + \mathrm{i}k\int_0^d \mathbf{N}(y)\mathrm{d}y + (\mathrm{i}k)^2\int_0^d \mathbf{N}(y)\mathrm{d}y\int_0^y \mathbf{N}(y_1)\mathrm{d}y_1 + \cdots \end{cases} \tag{10}$$

Introduce the 4×4 blocks of the 8×8 propagator $\mathbf{M}(d,0)$ and denote their similar to (3) partitioning as follows:

$$\mathbf{M}(d,0) = \begin{pmatrix} \mathbf{M}_1 & \mathbf{M}_2 \\ \mathbf{M}_3 & \mathbf{M}_4 \end{pmatrix},\quad \underset{i=1,\ldots,4}{\mathbf{M}_i} = \begin{pmatrix} \hat{\mathbf{m}}_i & \mathbf{l}_i \\ \mathbf{l}_i'^{\mathrm{T}} & g_i \end{pmatrix}, \tag{11}$$

where $\hat{\mathbf{m}}$, $\mathbf{l}$, and g are 3×3 matrices, vectors, and scalars, respectively. Applying the traction-free condition $\mathbf{F}(0)=\mathbf{0}$ and $\mathbf{F}(d)=\mathbf{0}$ at the plate faces and using (2_2), (9), (11) yields the dispersion equation

$$\det\left[\hat{\mathbf{m}}_3 - \frac{\left(\mathbf{l}_4 + \frac{\mathrm{i}}{\varepsilon_0^{(-)}}\mathbf{l}_3\right)\otimes\left(\mathbf{l}_1' + \frac{\mathrm{i}}{\varepsilon_0^{(+)}}\mathbf{l}_3'\right)}{g_2 + \frac{\mathrm{i}}{\varepsilon_0^{(-)}}g_1 + \frac{\mathrm{i}}{\varepsilon_0^{(+)}}g_4 - \frac{1}{\varepsilon_0^{(-)}\varepsilon_0^{(+)}}g_3}\right] = 0, \tag{12}$$

where $\hat{\mathbf{m}}_3 = \hat{\mathbf{m}}_3^{\mathrm{T}}$, $\mathbf{l}_1' = \mathbf{l}_4$, $\mathbf{l}_3 = \mathbf{l}_3'$, $g_1 = g_4$ if the plate is homogeneous. A detailed derivation of Eq. (12) can be found in Shuvalov et al. (2008). It is written in the form which incorporates different types of the electric boundary conditions (EBC), which are fixed by way of appropriate choice of the dielectric constants $\varepsilon_0^{(-)}$ and $\varepsilon_0^{(+)}$ of the exterior on both sides of the plate. The plate with non-metallized faces maintaining continuity of ϕ and D_y (which

then decrease away from the plate) implies setting $\varepsilon_0^{(-)} = \varepsilon_0^{(+)} = \varepsilon_0$. The plate with 'electrically closed' ($\phi = 0$) faces that are metallized and short-circuited is described by setting $\varepsilon_0^{(-)} = \varepsilon_0^{(+)} \to \infty$. A plate with one face, upper or lower, being metallized and the other face non-metallized corresponds, respectively, to $\varepsilon_0^{(-)} \to \infty$, $\varepsilon_0^{(+)} = \varepsilon_0$, or vice versa (both latter options are indeed equivalent for homogeneous plates; it is also so at the leading order in $kd \ll 1$ for functionally graded plates). Note that disregarding positive definiteness of the dielectric constant and formally taking zero $\varepsilon_0^{(\pm)}$ leads to another type of the 'closed' EBC: $D_y = 0$, which is not pursued in this paper.

By (2) and (10), $\mathbf{M}(d,0)$ expands in power series of kd with coefficients depending on v. Inserting this expansion by way of (11) into Eq. (12) and resolving it for v successively in each order of $kd \ll 1$ determines the Taylor series of three fundamental velocity branches $v_\alpha(k)$, $\alpha = 1, 2, 3$. In particular, $\mathbf{M}(d,0)$ truncated after $(kd)^2$-order enables finding the linear in kd slope of the flexural branch and the dispersion of the two upper fundamental branches to the quadratic order in $kd \ll 1$. The following explicit analysis is focussed on the coefficients of this long-wave expansion the fundamental branches $v_\alpha(k)$ (which can readily be recast to the equivalent form of low-frequency expansion of $v_\alpha(\omega)$ in powers of $\omega d/v_\alpha(0)$). The general procedure of deriving the coefficients in question is similar to the well-elaborated case of pure elasticity (e.g. Shuvalov, 2000; Poncelet et al., 2006); however, there is an essential difference which is that the piezoeffect lifts a restriction on $v^2(k)$ to expand in even powers of kd and hence permits a linear dispersion at the onset of the two upper fundamental branches. It is also noteworthy that taking an infinite or zero limit for $\varepsilon_0^{(\pm)}$, which enables easy re-adjustment of Eq. (12) from 'open' to 'closed' EBC, reshuffles the powers of kd in the dispersion equation and hence cannot be applied for the same purpose to the power-series solution $v(k)$ of (12).

3. Low-frequency dispersion in a homogeneous piezoplate

3.1. Flexural branch

Given an arbitrary anisotropic homogeneous piezoelectric plate, consider the leading-order dispersion at the onset of the flexural branch

$$v_1(k) = \kappa kd + \cdots (\Longleftrightarrow v_1(\omega) = \sqrt{\kappa \omega d} + \cdots). \tag{13}$$

We are concerned with the coefficient κ that defines the initial slope of the branch $v_1(k)$. Interestingly, κ is same for all types of the EBC in question, i.e. it does not depend on whether one or both faces are non-metallized or metallized. Its value is found to be

$$\kappa = \sqrt{\frac{1}{12\rho}\mathbf{m}\cdot\hat{\mathbf{n}}_3\mathbf{m}} = \sqrt{\kappa^{(\mathrm{els})^2} + \frac{(\mathbf{a}_1'\cdot\mathbf{m})^2}{12\rho b_2}} \text{ with}$$
$$\kappa^{(\mathrm{els})} = \sqrt{\frac{1}{12\rho}\mathbf{m}\cdot\mathbf{N}_3^{(\mathrm{els})}\mathbf{m}}, \tag{14}$$

where (4_3) was used to express κ via the well known evaluation of the slope $\kappa^{(\mathrm{els})}$ of the flexural branch $v_1^{(\mathrm{els})}(k)$ in the purely elastic plate. By (14),

$$\kappa \geqslant \kappa^{(\mathrm{els})}, \tag{15}$$

i.e. the piezoeffect either increases the initial slope of the flexural branch $v_1(k)$, or retains it when $\mathbf{a}_1'\cdot\mathbf{m} = 0$. In particular, $\kappa = \kappa^{(\mathrm{els})}$ for any propagation direction $\mathbf{m}$ in a plate which is either parallel to the symmetry plane m ($\mathbf{n} \perp m$), or orthogonal to the symmetry axis $\bar{6}$, or parallel to the basal plane of the axial symmetry group $G = 32$, 422 or 622, see Table in Appendix.

Fig. 2a,b demonstrates dependence of the flexural-branch slope κ on the orientation θ of the propagation direction $\mathbf{m} = \mathbf{m}(\theta)$ in the X_1-cut and X_2-cut $LiNBO_3$ plates (the material constants are taken from Dieulesaint and Royer, 1980). As noted above, the symmetry $3m$ of $LiNBO_3$ implies that $\kappa = \kappa^{(\mathrm{els})}$ for any θ in the X_1-cut where $\mathbf{n} \perp m$ (Fig. 2a), and $\kappa > \kappa^{(\mathrm{els})}$ for any θ in the X_2-cut which is neither parallel to a symmetry plane, nor orthogonal to a symmetry axis (Fig. 2b). According to (14_1), the dependence $\kappa(\theta)$ is governed by that of the quadratic form $\mathbf{m}\cdot\hat{\mathbf{n}}_3\mathbf{m}$ of the matrix $\hat{\mathbf{n}}_3(\theta)$. In particular, $\kappa(\theta)$ attains its extreme values, given by $\mathbf{m}\cdot\hat{\mathbf{n}}_3\mathbf{m} = \eta_\alpha(\theta)$, for the angles θ such that render $\mathbf{m}(\theta)$ parallel to $\mathbf{f}_\alpha(\theta)$, where η_α and $\mathbf{f}_\alpha \perp \mathbf{n}$ ($\alpha = 2,3$) are the eigenvalues and eigenvectors of $\hat{\mathbf{n}}_3$, see (7). Further general analysis, resting on the aggregate zero or $\pm 2\pi$ rotation of the frame $\mathbf{f}_2(\theta) \perp \mathbf{f}_3(\theta)$ as $\mathbf{m}(\theta)$ makes a complete circle about the given $\mathbf{n}$, can be developed similarly to Shuvalov (1999). It is, however, obvious that if the planar anisotropy is not very strong, then the shape of the curve $\kappa(\theta)$ is close enough to that of the square root of the eigenvalue $\eta_3(\theta) > \eta_2(\theta)$ associated with the quasi-longitudinal eigenbranch of $\hat{\mathbf{n}}_3(\theta)$. This is observed on comparing the curves $\kappa(\theta)$ in Fig. 2a,b to the curves $v = \sqrt{\eta_3(\theta)/\rho}$ in Fig. 4b and Fig. 5b, which are displayed and discussed below (Section 3.2.3).

In contrast to other anisotropic plate settings, the coefficient κ in a trigonal or cubic plate with the normal $\mathbf{n}\|3$ is independent of the orientation of $\mathbf{m}$. This is because any $\mathbf{m}(\theta) \perp 3$ is the (longitudinal) eigenvector of $\hat{\mathbf{n}}_3(\theta)$ corresponding to a constant eigenvalue $\mathbf{m}\cdot\hat{\mathbf{n}}_3\mathbf{m} \equiv \eta_L$. Therefore $\kappa = \sqrt{\eta_L/12\rho} = const$ for any θ. Its explicit form specifies by appeal to Section A.1 of Appendix as

$$\kappa = \sqrt{\kappa^{(\mathrm{els})^2} + \frac{(e_{31} - e_{33}c_{13}/c_{33})^2}{12\rho(\varepsilon_{33} + e_{33}^2/c_{33})}} \text{ with}$$
$$\kappa^{(\mathrm{els})} = \sqrt{\frac{1}{12\rho}\left(c_{11} - \frac{c_{13}^2}{c_{33}} - \frac{c_{14}^2 + c_{25}^2}{c_{44}}\right)}. \tag{16}$$

Such isotropy of the leading-order coefficient κ in the plane, which is not a plane of transverse isotropy of itself, does not indeed extend to the whole flexural branch $v_1(k)$.

By analogy with Mindlin's approximation for purely elastic plates (see Poncelet et al., 2006 for the details), knowing κ can be used for fitting a full extent of the flexural branch $v_1(k)$ as follows

$$v_1(k) \approx \frac{\kappa kd}{\sqrt{1 + (\kappa kd)^2/v_{\mathrm{SAW}}^2}}, \tag{17}$$

where v_{SAW} is the value of surface wave velocity along $\mathbf{m}$ which is approached by $v_1(k)$ at high frequency. Fig. 2c shows the flexural branch and its approximation (17) with κ given by (16) for the X_3-cut $LiNBO_3$ plate. Note that the numerical difference between the actual slope κ and its 'purely elastic' value $\kappa^{(\mathrm{els})}$ happens to be very small ($\sim 10^{-3}$). For a comparison, Fig. 2d demonstrates the flexural-branch onset for the same geometry in the PMN–33%PT plate (the material constants are taken from Zhang et al., 2003), for which Eq. (16) gives $\kappa \approx 0.997$ while $\kappa^{(\mathrm{els})} \approx 0.817$.

Finally, note that the displacement amplitude of the flexural wave taken to the first order in kd remains not piezoactive:

$$\mathbf{A}_1(y) = \mathbf{n} - \mathrm{i}k\mathbf{m}(y - d/2). \tag{18}$$

All the other amplitudes $\mathrm{i}k^{-1}\mathbf{F}_1$, ϕ_1, $\mathrm{i}k^{-1}D_y$ constituting the state vector $(2)_2$ for the flexural wave are of the leading order $(kd)^2$.

3.2. Upper fundamental branches

3.2.1. Arbitrary anisotropy

Consider the low-frequency long-wave dispersion of the two upper fundamental velocity branches in a homogeneous piezoelectric plate,

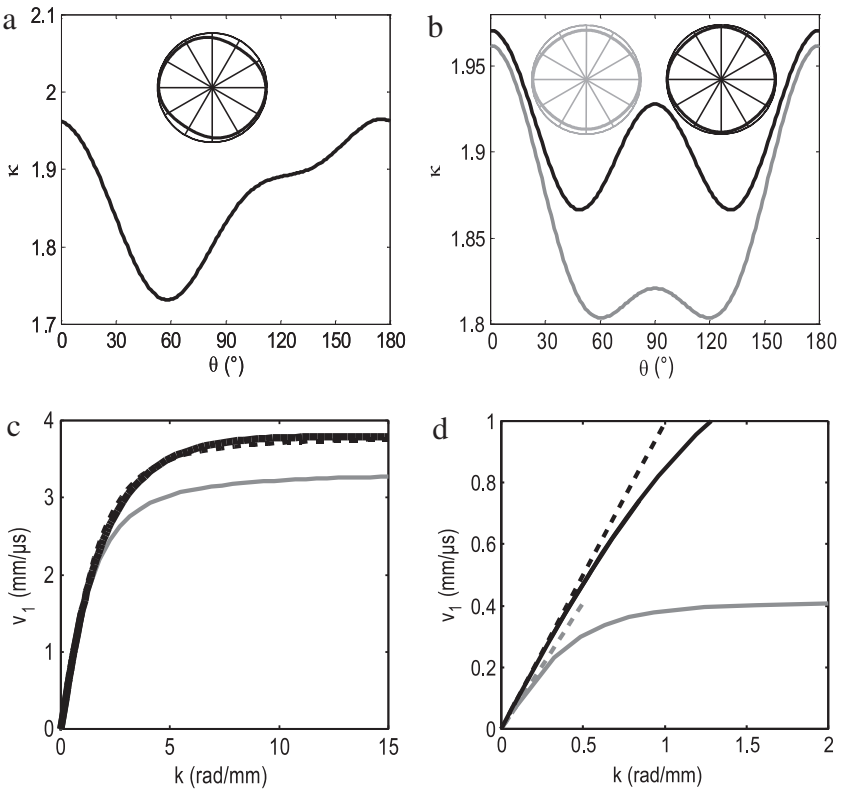

Fig. 2. Azimuthal variation of the flexural-branch slope $\kappa(\theta)$ (14) in the (a) X_1-cut and (b) X_2-cut $LiNBO_3$ plates. The angle θ is counted from $X_3\|3$ (as in (50)). In the case (a), $\kappa = \kappa^{(\mathrm{els})}$; in the case (b), κ and $\kappa^{(\mathrm{els})}$ are displayed by black and grey lines, respectively. Fig. (c) shows the exact flexural branch $v_1(k)$ (black line) and its the approximation (17) (dashed line) for the propagation direction $\mathbf{m}\|X_1$ in the X_3-cut $LiNBO_3$ plate; the grey line is the same branch computed without account for piezoeffect. Fig. (d) shows the flexural-branch onset with and without account for piezoeffect (black and grey lines, respectively) for the X_3-cut PMN–33%PT plate; the slopes evaluated by (16) are indicated by a dashed line.

$$v_\alpha(k) = v_{0\alpha}[1 + B_\alpha(kd) + C_\alpha(kd)^2 + \cdots], \quad \alpha = 2,3. \tag{19}$$

Note that (19) can be recast to the form $v_\alpha(\omega)$ by replacing k with $\omega/v_{0\alpha}$ and C_α with $C_\alpha - B_\alpha^2$. The zero-order velocities $v_{0\alpha}$ and the dispersion coefficients B_α, C_α generally depend on the type of EBC and thus need to be labeled accordingly. In the following we use the superscript $^{(\mathrm{f/f})}$ for a non-metallized (free of charge) plate, $^{(\mathrm{f/m})}$ for a plate with one face metallized, and $^{(\mathrm{m/m})}$ for a plate with metallized and short-circuited faces; while, as before, $^{(\mathrm{els})}$ indicates the purely elastic case.

The zero-order velocity $v_{0\alpha}$ and polarization vector $\mathbf{A}_{0\alpha}$ corresponding to the ω, $k \to 0$ limit are given by the eigenvalues and eigenvectors (7) of either $\hat{\mathbf{n}}_3$ or $\mathbf{N}_3^{(\mathrm{els})}$, the choice depending on the type of EBC as follows:

$$\begin{aligned} &v_{0\alpha}^{(\mathrm{f/f})} = v_{0\alpha}^{(\mathrm{f/m})} = \sqrt{\eta_\alpha/\rho}, \quad v_{0\alpha}^{(\mathrm{m/m})} = \sqrt{\eta_\alpha^{(\mathrm{els})}/\rho}\left(= v_{0\alpha}^{(\mathrm{els})}\right); \\ &\mathbf{A}_{0\alpha}^{(\mathrm{f/f})} = \mathbf{A}_{0\alpha}^{(\mathrm{f/m})} = \mathbf{f}_\alpha, \quad \mathbf{A}_{0\alpha}^{(\mathrm{m/m})} = \mathbf{f}_\alpha^{(\mathrm{els})}\left(= \mathbf{A}_{0\alpha}^{(\mathrm{els})}\right), \quad \alpha = 2,3. \end{aligned} \tag{20}$$

The linear-dispersion coefficients B_α are

$$\begin{aligned} &B_\alpha^{(\mathrm{f/f})} = \frac{1}{4\eta_\alpha}\left[\frac{(\mathbf{a}_3\cdot\mathbf{f}_\alpha)^2}{\varepsilon_0} - \varepsilon_0\left(\mathbf{a}_1'\cdot\mathbf{f}_\alpha\right)^2\right]; \\ &B_\alpha^{(\mathrm{f/m})} = -\frac{\varepsilon_0\left(\mathbf{a}_1'\cdot\mathbf{f}_\alpha\right)^2}{2\eta_\alpha}; \quad B_\alpha^{(\mathrm{m/m})} = 0, \quad \alpha = 2,3, \end{aligned} \tag{21}$$

where sign of B_α is set w.r.t. $k > 0$ as understood hereafter. By the definition (4) of the vectors $\mathbf{a}_1'$ and $\mathbf{a}_3$, the coefficients $B_\alpha^{(\mathrm{f/f})}$ and $B_\alpha^{(\mathrm{f/m})}$ in a non-metallized and one-side metallized plate are of the order of the piezoelectric-coupling parameter $e^2/\varepsilon c$. Due to $B_\alpha^{(\mathrm{m/m})} = 0$, the leading-order dispersion (19) in a short-circuited plate is quadratic in kd (the same holds true for the model type of EBC $D_y = 0$, see Wu et al., 2005). The quadratic-dispersion coefficient $C_\alpha^{(\mathrm{m/m})}$ is

$$\begin{aligned} &C_\alpha^{(\mathrm{m/m})} = C_\alpha^{(\mathrm{els})} + \frac{1}{24\eta_\alpha^{(\mathrm{els})}b_2}\left[\left(b_2\mathbf{a}_3 + \mathbf{N}_1^{(\mathrm{els})\mathrm{T}}\mathbf{a}_1' - b_1\mathbf{a}_1'\right)\cdot\mathbf{f}_\alpha^{(\mathrm{els})}\right]^2 \\ &\text{with } C_\alpha^{(\mathrm{els})} = \frac{1}{24\eta_\alpha^{(\mathrm{els})}}\mathbf{f}_\alpha^{(\mathrm{els})}\cdot\mathbf{N}_1^{(\mathrm{els})\mathrm{T}}\left(\mathbf{N}_3^{(\mathrm{els})} - \eta_\alpha^{(\mathrm{els})}\mathbf{I}\right)\mathbf{N}_1^{(\mathrm{els})}\mathbf{f}_\alpha^{(\mathrm{els})}, \quad \alpha = 2,3. \end{aligned} \tag{22}$$

Expressions of $C_\alpha^{(\mathrm{f/f})}$ and $C_\alpha^{(\mathrm{f/m})}$ for generally anisotropic plates are rather lengthy and therefore omitted. Benchmarks of the zero- and first-order parameters (20) and (21) for various plate orientations are listed in Table in Appendix.

Eqs. (20)–(22) (see also (8)) enable the following general observations on the onset of the upper fundamental branches $v_\alpha(k)$, $\alpha = 2, 3$, in an arbitrary anisotropic homogeneous piezoelectric plate.

- The hierarchy of the zero-order velocity values $v_{0\alpha}$ is

$$\begin{aligned} v_{03}^{(\mathrm{f/f})} = v_{03}^{(\mathrm{f/m})} \geqslant v_{03}^{(\mathrm{m/m})} = v_{03}^{(\mathrm{els})} \geqslant v_{02}^{(\mathrm{f/f})} = v_{02}^{(\mathrm{f/m})} \\ \geqslant v_{02}^{(\mathrm{m/m})} = v_{02}^{(\mathrm{els})}. \end{aligned} \tag{23}$$

  Note that, for any fixed propagation direction $\mathbf{m}$, the velocity increment occurring due to the piezoelectric coupling cannot yet lead to $\min_{\alpha=2,3}\{v_{0\alpha}\} > \max_{\alpha=2,3}\{v_{0\alpha}^{(\mathrm{els})}\}$.
- The linear onset of the branches $v_{2,3}(k)$ in a metallized short-circuited plate remains disallowed like for the elastic plates: $B_\alpha^{(\mathrm{m/m})} = B_\alpha^{(\mathrm{els})} = 0$. By contrast, if one or both faces are non-metallized, then the linear dispersion is generally non-zero and proportional to piezoelectric coupling. The coefficient $B_\alpha^{(\mathrm{f/f})}$ is not sign-definite but is always greater or equal than the coefficient $B_\alpha^{(\mathrm{f/m})}$ which is non-positive:

$$B_\alpha^{(\mathrm{f/f})} \geqslant B_\alpha^{(\mathrm{f/m})}, \quad B_\alpha^{(\mathrm{f/m})} \leqslant 0. \tag{24}$$

- Let $v_3^{(\mathrm{els})}(k)$ in a purely elastic homogeneous plate satisfy $v_{03}^{(\mathrm{els})} > v_{02}^{(\mathrm{els})}$ if both $v_{2,3}^{(\mathrm{els})}(k)$ are dispersive, otherwise let $v_3^{(\mathrm{els})}(k)$ be the in-plane polarized branch if $\{\mathbf{m},\mathbf{n}\}$ is a symmetry plane (where the other branch is SH_0 $v_2^{(\mathrm{els})} = const$). The onset of $v_3^{(\mathrm{els})}(k)$ is known to always go downwards, in consequence of the theorem stating that $v_{03}^{(\mathrm{els})}$ is an invariant bound, above which all the branches $v^{(\mathrm{els})}(k)$ of the given plate spectrum are decreasing (Shuvalov, 2004; Shuvalov, 2006). None of these properties are generally valid for a non-metallized piezoelectric plate due to possibly positive $B_\alpha^{(\mathrm{f/f})}$.
- For a plate with short-circuited faces, the coefficient of leading-order (quadratic) dispersion is always greater or equal than its value calculated without regard for piezoeffect,

$$C_\alpha^{(\mathrm{m/m})} \geqslant C_\alpha^{(\mathrm{els})}. \tag{25}$$

3.2.2. Plate orthogonal to the threefold axis ($\mathbf{n}\|3$)

Consider a piezoelectric plate which is cut orthogonally to the threefold axis 3 (see Section A.1 of Appendix). The zero-order velocity $v_{0\alpha}$ and polarization $\mathbf{A}_{0\alpha}$ (20) for such a plate are isotropic, i.e., $v_{0\alpha}$ is the same and $\mathbf{A}_{0\alpha}(\perp\mathbf{n})$ is pure longitudinal and transverse for any azimuthal orientation of the propagation direction $\mathbf{m} = \mathbf{m}(\theta)$. It is therefore suitable to replace the branch labels

$$\alpha = 2,3 \Rightarrow \alpha = T, L, \tag{26}$$

so that $\mathbf{A}_{0T}\|\mathbf{t} = \mathbf{n}\times\mathbf{m}$ and $\mathbf{A}_{0L}\|\mathbf{m}$. The given plate normal $\mathbf{n}\|3$ implies $\mathbf{a}_1' = \mathbf{0}$ for plates of the 32 class and $\mathbf{a}_1'\|\mathbf{m}$ for other trigonal or cubic piezoplates. In the former case, by (4), the matrix $\hat{\mathbf{n}}_3$ coincides with $\mathbf{N}_3^{(\mathrm{els})}$ and so the zero-order velocity is not piezoactive for both branches: $v_{0\alpha}^{(\mathrm{f/f})} = v_{0\alpha}^{(\mathrm{els})}$, $\alpha = T, L$. In the latter case, the longitudinal wave velocity is piezoactive whereas transverse wave velocity is not: $v_{0L}^{(\mathrm{f/f})} > v_{0L}^{(\mathrm{els})}$ and $v_{0T}^{(\mathrm{f/f})} = v_{0T}^{(\mathrm{els})}$.

Assume the plate material of the class $G = 3m$ and set $X_3\|3$. As mentioned above, $v_{0T}^{(\mathrm{f/f})} = \sqrt{\eta_T/\rho}$ and $v_{0L}^{(\mathrm{f/f})} = \sqrt{\eta_L/\rho}$ are defined through the eigenvalues of $\hat{\mathbf{n}}_3$ that are constant (independent of θ) and have an explicit form

$$\eta_T = \eta_T^{(\mathrm{els})} = c_{66} - \frac{c_{14}^2}{c_{44}}; \quad \eta_L = \eta_L^{(\mathrm{els})} + \frac{a_1'^2}{b_2},$$
$$\eta_L^{(\mathrm{els})} = c_{11} - \frac{c_{13}^2}{c_{33}} - \frac{c_{14}^2}{c_{44}}. \tag{27}$$

The coefficients (21) of linear dispersion for the non-metallized and one-side metallized plate are

$$B_T^{(\mathrm{f/f})}(\theta) = \frac{a_3^2\cos^2 3\theta}{4\varepsilon_0\eta_T^{(\mathrm{els})}}, \quad B_L^{(\mathrm{f/f})}(\theta) = \frac{1}{4\eta_L}\left(\frac{a_3^2\sin^2 3\theta}{2\varepsilon_0} - \varepsilon_0 a_1'^2\right);$$
$$B_T^{(\mathrm{f/m})} = 0, \quad B_L^{(\mathrm{f/m})} = -\frac{\varepsilon_0 a_1'^2}{2\eta_L}. \tag{28}$$

The coefficients (22) of the leading-order (quadratic) dispersion for the short-circuited plate are

$$C_T^{(\mathrm{m/m})}(\theta) = C_T^{(\mathrm{els})} + \frac{1}{24\eta_T^{(\mathrm{els})}}\left(\frac{c_{14}}{c_{44}}\right)^2\frac{a_1'^2}{b_2}\cos^2 3\theta,$$
$$C_L^{(\mathrm{m/m})}(\theta) = C_L^{(\mathrm{els})} - \frac{1}{24\eta_L^{(\mathrm{els})}b_2}\left(b_2a_3 + \frac{c_{14}}{c_{44}}a_1'\right)^2\sin^2 3\theta,$$
$$\text{where}: \ C_T^{(\mathrm{els})}(\theta) = \frac{1}{24}\left(\frac{c_{14}}{c_{44}}\right)^2\left(\frac{\eta_L^{(\mathrm{els})}}{\eta_T^{(\mathrm{els})}} - 1\right)\cos^2 3\theta,$$
$$C_L^{(\mathrm{els})}(\theta) = -\frac{1}{24}\left[\left(\frac{c_{13}}{c_{33}}\right)^2 + \left(1 - \frac{\eta_T^{(\mathrm{els})}}{\eta_L^{(\mathrm{els})}}\right)\left(\frac{c_{14}}{c_{44}}\right)^2\cos^2 3\theta\right]. \tag{29}$$

In the above expressions, the azimuth θ is counted from $X_1 \perp m$ and

$$b_2 = \frac{1}{\varepsilon_{33} + e_{33}^2/c_{33}}, \quad a_1' = \frac{e_{31}c_{33} - e_{33}c_{13}}{\varepsilon_{33}c_{33} + e_{33}^2}, \quad a_3 = e_{22} + \frac{e_{15}c_{14}}{c_{44}}. \tag{30}$$

Lengthy expressions for $C_\alpha^{(\mathrm{f/f})}$ and $C_\alpha^{(\mathrm{f/m})}$ are omitted.

Fig. 3a-d shows the angular dependence of the coefficients of linear and quadratic dispersion $B_{T,L}^{(\mathrm{f/f})}(\theta)$ and $C_{T,L}^{(\mathrm{f/f})}(\theta)$ in the non-metallized X_3-cut $LiNbO_3$ plate. The zero-order (for $k = 0$) velocities $v_{0T}^{(\mathrm{f/f})}$ and $v_{0L}^{(\mathrm{f/f})}$ are not presented since they are independent of θ, see (27). Moreover, $v_{0L}^{(\mathrm{f/f})}$ is almost not piezoactive for the case in hand due to a numerically small term $a_1'^2/b_2$ in (27). According to Eq. ($28_{1,2}$), the linear-dispersion coefficients $B_T^{(\mathrm{f/f})}(\theta)$ and $B_L^{(\mathrm{f/f})}(\theta)$ have maximum values for the periodically repeated orientations $\theta = 0$ and $\theta = 30^\circ$ of $\mathbf{m}(\theta)$, respectively. These are the orientations for which the unusual, linear trend of the long-wave dispersion of one or the other branch $v_T(k)$, $v_L(k)$ is most prominent. Correspondingly, since the linear dispersion is entirely due to the piezoeffect, these orientations yield the most noticeable departure of the long-wave onset of the exact dispersion curve $v_T(k)$ or $v_L(k)$ from its 'would-be' shape that disregards the piezoeffect. This is demonstrated in Fig. 3e,f. Note that $v_{0L}^{(\mathrm{f/f})} \approx v_{0L}^{(\mathrm{els})}$ as mentioned above. Also note that the linear dispersion of $v_L(k)$ is lessened in the present case due to the fact that $B_L^{(\mathrm{f/f})}$ given in (28) contains two terms of the opposite sign (cf. (32)). At the same time, comparing the values of $B_{T,L}^{(\mathrm{f/f})}(\theta)$ and $C_{T,L}^{(\mathrm{f/f})}(\theta)$ ($\alpha = T, L$) displayed in 3a,b and c,d reveals that a general predominance of the linear over the quadratic dispersion in small kd is enhanced by the overall numerical predominance of the corresponding coefficients $B_{T,L}^{(\mathrm{f/f})}$ over $C_{T,L}^{(\mathrm{f/f})}$. This feature is also typical for other orientations of the $LiNbO_3$ plate, see Figs. 4,5 below.

3.2.3. Plate parallel to the symmetry plane m ($\mathbf{n} \perp m$)

If a piezoelectric plate is cut along the symmetry plane m, then $\mathbf{a}_1' = \mathbf{0}$ and hence, for any propagation direction $\mathbf{m} = \mathbf{m}(\theta)$ in m, the limit $\omega, k \to 0$ of both upper fundamental branches $v_\alpha(k)$ is not affected by the piezoelectric coupling:

$$v_{0\alpha}^{(\mathrm{f/f})}(\theta) = \sqrt{\eta_\alpha^{(\mathrm{els})}(\theta)/\rho} = v_{0\alpha}^{(\mathrm{els})}(\theta),$$
$$\mathbf{A}_{0\alpha}^{(\mathrm{f/f})}(\theta) = \mathbf{f}_\alpha^{(\mathrm{els})}(\theta) = \mathbf{A}_{0\alpha}^{(\mathrm{els})}(\theta), \tag{31}$$

where $\alpha = 2, 3$ (chosen so that $v_{02} < v_{03}$ for a given θ). The coefficients (21) of linear dispersion reduce to the form

$$B_\alpha^{(\mathrm{f/f})}(\theta) = \frac{(\mathbf{a}_3\cdot\mathbf{f}_\alpha^{(\mathrm{els})})^2}{4\varepsilon_0\eta_\alpha^{(\mathrm{els})}} (\geqslant 0), \quad B_\alpha^{(\mathrm{f/m})} = 0. \tag{32}$$

The coefficients of the quadratic dispersion are

$$C_\alpha^{(\mathrm{f/f})}(\theta) = C_\alpha^{(\mathrm{els})} + \frac{\left(\mathbf{a}_3\cdot\mathbf{f}_\alpha^{(\mathrm{els})}\right)^2}{8\eta_\alpha^{(\mathrm{els})}}\left[\frac{b_2}{3} - \frac{1}{\varepsilon_0} + \frac{b_3}{\varepsilon_0^2} + \frac{\left(\mathbf{a}_3\cdot\mathbf{f}_\beta^{(\mathrm{els})}\right)^2}{\varepsilon_0^2\left(\eta_\alpha^{(\mathrm{els})} - \eta_\beta^{(\mathrm{els})}\right)}\right]$$
$$(\alpha,\beta = 2,3, \ \alpha \neq \beta);$$

$$C_\alpha^{(\mathrm{f/m})}(\theta) = C_\alpha^{(\mathrm{els})} + \frac{b_2\left(\mathbf{a}_3\cdot\mathbf{f}_\alpha^{(\mathrm{els})}\right)^2}{6\eta_\alpha^{(\mathrm{els})}}$$
$$\geqslant C_\alpha^{(\mathrm{m/m})}(\theta) = C_\alpha^{(\mathrm{els})} + \frac{b_2\left(\mathbf{a}_3\cdot\mathbf{f}_\alpha^{(\mathrm{els})}\right)^2}{24\eta_\alpha^{(\mathrm{els})}}$$
$$\geqslant C_\alpha^{(\mathrm{els})}(\theta) = -\frac{\left(\mathbf{n}\cdot\mathbf{N}_1^{(\mathrm{els})}\mathbf{f}_\alpha^{(\mathrm{els})}\right)^2}{24}. \tag{33}$$

The entries of these equations are detailed in Section A.2 of Appendix.

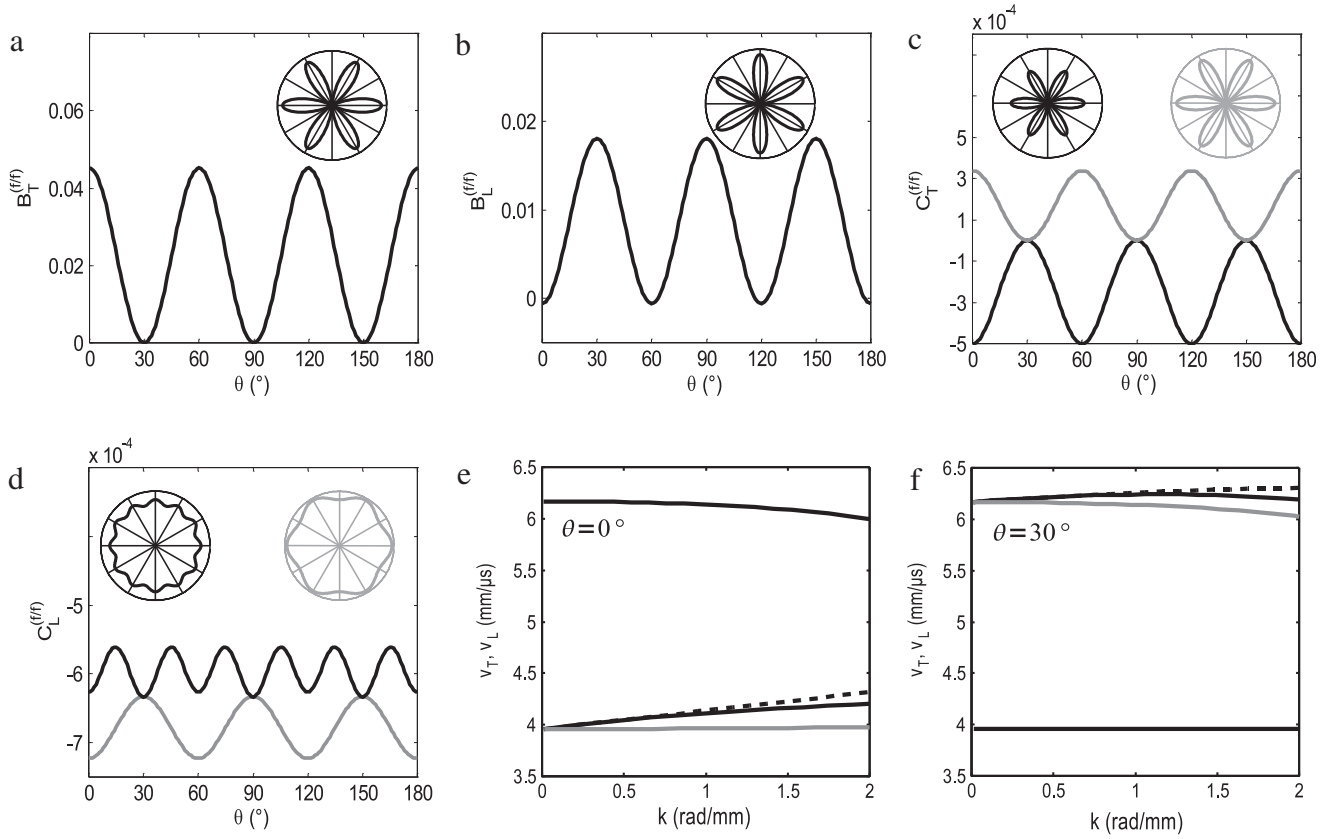

Fig. 3. Azimuthal variation of the coefficients of (a,b) linear dispersion $B_{T,L}^{(f/f)}(\theta)$ and (c,d) quadratic dispersion $C_{T,L}^{(f/f)}(\theta)$ at the long-wave onset of (quasi-) transverse and longitudinal branches $v_{T,\,L}(k)$ in the non-metallized X_3-cut $LiNbO_3$ plate. The angle θ is counted from $X_1 \perp m$ (as in (47)). Black and grey lines show the evaluation with and without account for piezoeffect, respectively; the polar diagrams display the absolute values. Figs. (e) and (f) zoom in on the branches $v_T(k) < v_L(k)$ plotted for $\theta = 0$ and $\theta = 30°$; here black and grey lines show the results of exact calculation with and without account for piezoeffect, and the dashed line demonstrates the asymptotics (19) with the found coefficients (due to the scale, the grey and dashed lines merge with the black ones for v_L in (e) and for v_T in (f)).

Fig. 4a-f shows the azimuthal variation of the above-defined zero-order velocity $v_{0\alpha}^{(f/f)}(\theta)$ and dispersion coefficients $B_\alpha^{(f/f)}(\theta)$ and $C_\alpha^{(f/f)}(\theta)$ in the non-metallized X_1-cut $LiNbO_3$ plate. In difference to the case of X_3-cut (Section 3.2.2), the velocity values at the $\omega, k \to 0$ limit are anisotropic: $v_{0\alpha}^{(f/f)} = v_{0\alpha}^{(f/f)}(\theta)$, see Fig. 4a,b. A similarity of the shape of the curve $v_{03}^{(f/f)}(\theta)$ (Fig. 4b) to that of the curve $\kappa(\theta)$ for the flexural-branch slope (Fig. 2a) has been explained in Section 3.1. From Fig. 4c,d, it is seen that each of the linear-dispersion coefficients $B_2^{(f/f)}(\theta)$ and $B_3^{(f/f)}(\theta)$ caused by the piezocoupling has a distinctive peak with a maximum near $\theta = 90°$ and $\theta = 60°$, respectively, and is relatively small away from this peak. Such 'angular selectivity' of the effect of piezocoupling is in agreement with the numerical modelling reported for the X_1-cut $LiNbO_3$ plate in Yang and Chimenti (1995), Yang and Huang (2003), where the linear trend at the onset of branches $v_2^{(f/f)}(k)$ and $v_3^{(f/f)}(k)$ clearly shows up for the propagation directions $\mathbf{m}(\theta)$ restricted to the sector $\Delta\theta \approx \pm 15°$ about, respectively, $\theta = 90°$ and $\theta = 60°$ (the present notation θ for the azimuth angle corresponds to $\psi = \theta$ in Yang and Chimenti (1995) and to $\Phi = \pi/2 + \theta$ in Yang and Huang (2003)). The long-wave dispersion curves $v_{2,3}^{(f/f)}(k)$ for $\theta = 90°$ and $\theta = 60°$ and the comparison with their 'would-be' shape $v_\alpha^{(els)}(k)$ in disregard of piezoelectricity are demonstrated in Fig. 4g,h.

For completeness, Fig. 5 presents the same results for the non-metallized X_2-cut $LiNbO_3$ plate. In this case, the zero-order velocity $v_{0\alpha}^{(f/f)}(\theta)$ for both branches $\alpha = 2, 3$ can be piezoactive. Fig. 5a,b shows that the maximum effect of piezocoupling at $\omega, k \to 0$ is observed for the upper velocity $v_{03}^{(f/f)}$ at $\theta = 90°$. As in the previous cases, the linear-dispersion coefficients $B_\alpha^{(f/f)}(\theta)$ (Fig. 5c,d) are in general greater than the quadratic-dispersion coefficients $C_\alpha^{(f/f)}(\theta)$ (Fig. 5e,f). Angular dependence of $B_\alpha^{(f/f)}(\theta)$ is similar to that in Fig. 4c,d in that it has a relatively narrow extremum. It occurs for both branches at $\theta = 90°$ as a maximum for $\alpha = 2$ and a numerically less distinctive minimum for $\alpha = 3$. The resulting linear trend of the long-wave dispersion curves $v_{2,3}^{(f/f)}(k)$ for $\theta = 90°$ is demonstrated in Fig. 5g (where the dashed black and grey lines display the asymptotics (19) with and without account for piezoeffect, respectively).

3.2.4. Plate orthogonal to the twofold axis 2 ($\mathbf{n} \| 2$)

Pure elastic wave parameters of this case are the same as in the above case $\mathbf{n} \perp m$ but the piezoelectric properties are different. Now $\mathbf{a}_3 = \mathbf{0}$ for any orientation θ of $\mathbf{m}$ (θ), while the vector $\mathbf{a}_1'$ is generally non-zero and hence $\hat{\mathbf{n}}_3 \neq \mathbf{N}_3^{(els)}$. Therefore the zero-order limit $v_{0\alpha}^{(f/f)}$ of the upper fundamental branches $v_\alpha^{(f/f)}(k)$, $\alpha = 2, 3$, in a non-metallized plate with the normal $\mathbf{n} \| 2$ is generally piezoactive, as given by (20) with $\eta_\alpha(\theta)$, $\mathbf{f}_\alpha(\theta) \neq \eta_\alpha^{(els)}$, $\mathbf{f}_\alpha^{(els)}(\theta)$. The linear- and quadratic-dispersion coefficients are as follows:

$$B_\alpha^{(f/f)}(\theta) = -\frac{\varepsilon_0 \left(\mathbf{a}_1' \cdot \mathbf{f}_\alpha\right)^2}{4\eta_\alpha} = \frac{1}{2} B_\alpha^{(f/m)}(\theta) \leqslant 0;$$

$$C_\alpha^{(f/f)}(\theta) = C_\alpha^{(els)} + \frac{\left(\mathbf{a}_1' \cdot \mathbf{f}_\alpha\right)^2}{8\eta_\alpha}\left[\frac{b_3}{3} + \frac{1}{\varepsilon_0} + \varepsilon_0^2 b_2 + \frac{\varepsilon_0^2 \left(\mathbf{a}_1' \cdot \mathbf{f}_\beta\right)^2}{\eta_\alpha - \eta_\beta}\right],$$

$$C_\alpha^{(f/m)}(\theta) = C_\alpha^{(els)} + \frac{\left(\mathbf{a}_1' \cdot \mathbf{f}_\alpha\right)^2}{2\eta_\alpha}\left[\frac{b_3}{3} + \varepsilon_0^2 b_2 + \frac{\varepsilon_0^2 \left(\mathbf{a}_1' \cdot \mathbf{f}_\beta\right)^2}{\eta_\alpha - \eta_\beta}\right],$$

$$C_\alpha^{(m/m)}(\theta) = C_\alpha^{(els)}(\theta) = -\frac{\left(\mathbf{n} \cdot \mathbf{N}_1^{(els)} \mathbf{f}_\alpha^{(els)}\right)^2}{24}, \qquad (34)$$

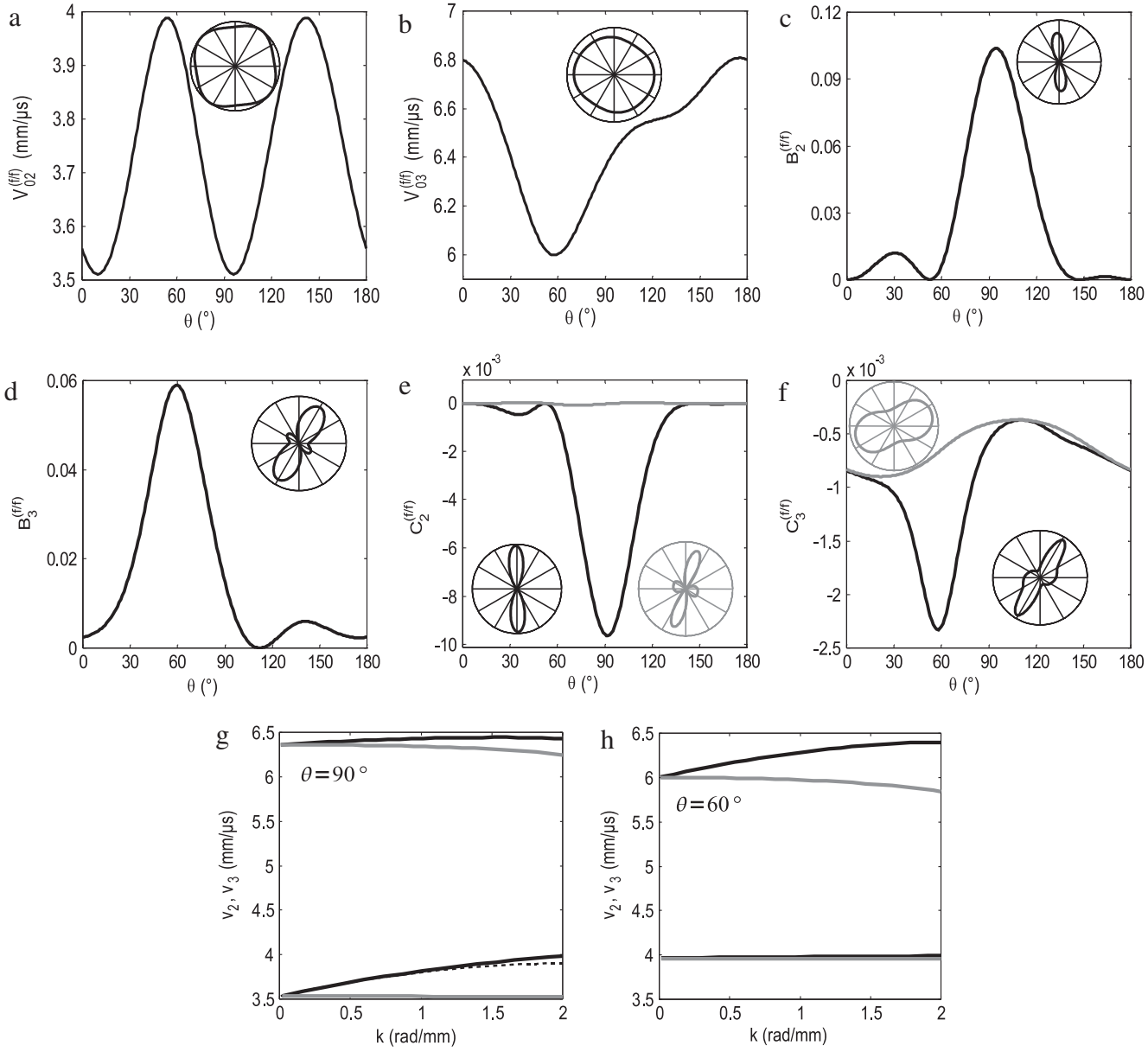

Fig. 4. Azimuthal variation of (a,b) the zero-order velocity $v_{0\alpha}^{(f/f)}(\theta)\left(=v_{0\alpha}^{(els)}(\theta)\right)$, (c,d) linear-dispersion coefficients $B_\alpha^{(f/f)}(\theta)$, and (e,f) quadratic-dispersion coefficients $C_\alpha^{(f/f)}(\theta)$ at the long-wave onset of the upper fundamental branches $v_\alpha(k)$ ($\alpha=2,3$) in the non-metallized X_1-cut $LiNbO_3$ plate. The angle θ is counted from $X_3\|3$. Figs. (g) and (h) zoom in on the branches $v_{2,3}(k)$ plotted for $\theta=90°$ and $\theta=60°$. The polar diagrams in (a)–(f) display the absolute values; the black and grey lines show the exact evaluation with and without account for piezoeffect, respectively. To the scale of (g) and (e), the asymptotics (19) with the found coefficients (see Eqs. (31)–(33)) merge with the exact data except for v_2 in (g) where (19) is shown by a dashed line.

where $\alpha,\beta=2,3$, $\alpha\neq\beta$. For more explicit details, see Section A.2 of Appendix.

4. Functionally graded plate

4.1. Averaged auxiliary matrices

Consider a functionally graded (FG) plate with material properties depending on y. Denote their averaging through the plate thickness by the symbol

$$\langle\cdots\rangle=\frac{1}{d}\int_0^d\ldots\mathrm{d}y=\int_0^1\ldots\mathrm{d}\varsigma,\ \text{where}\ \varsigma=\frac{y}{d}. \tag{35}$$

In the following, the anisotropic quantities are written without an explicit reference to the azumuth angle θ of $\mathbf{m}(\theta)$ as their argument. The leading order of the low-frequency long-wave approximation in elastic FG plates is based on the Stroh block $\mathbf{N}_3^{(els)}(y)$ and on its through-plate average (e.g. Zakharov and Becker, 2000; Shuvalov et al., 2005). The impact of piezoeffect brings in the matrix $\hat{\mathbf{n}}_3(y)=\mathbf{N}_3^{(els)}-\frac{1}{b_2}\mathbf{a}_1'\otimes\mathbf{a}_1'$ and also another matrix $\tilde{\mathbf{n}}_3(y)$,

$$\tilde{\mathbf{n}}_3(y)=\hat{\mathbf{n}}_3-\frac{\mathbf{a}_1'\otimes\langle\mathbf{a}_1'\rangle}{\langle b_2\rangle}=\tilde{\mathbf{n}}_3^{\mathrm{T}},\quad\langle\tilde{\mathbf{n}}_3\rangle=\langle\hat{\mathbf{n}}_3\rangle-\frac{1}{\langle b_2\rangle}\langle\mathbf{a}_1'\rangle\otimes\langle\mathbf{a}_1'\rangle, \tag{36}$$

where $b_2(y)>0$ and $\mathbf{a}_1'(y)\cdot\mathbf{n}=0$ (see (6)). Each of the averaged matrices $\langle\mathbf{N}_3^{(els)}\rangle$, $\langle\hat{\mathbf{n}}_3\rangle$ and $\langle\tilde{\mathbf{n}}_3\rangle$ is symmetric and has a null vector $\mathbf{n}$. Denote the remaining eigen-pairs as follows:

$$\left\langle\mathbf{N}_3^{(els)}\right\rangle\bar{\mathbf{f}}_\alpha^{(els)}=\bar{\eta}_\alpha^{(els)}\bar{\mathbf{f}}_\alpha^{(els)};\quad\langle\hat{\mathbf{n}}_3\rangle\bar{\mathbf{f}}_\alpha=\bar{\eta}_\alpha\bar{\mathbf{f}}_\alpha;\quad\langle\tilde{\mathbf{n}}_3\rangle\bar{\mathbf{g}}_\alpha=\bar{\mu}_\alpha\bar{\mathbf{g}}_\alpha,\quad\alpha=2,3. \tag{37}$$

For any fixed θ, the eigenvalues (37) numbered in the increasing order satisfy the inequality

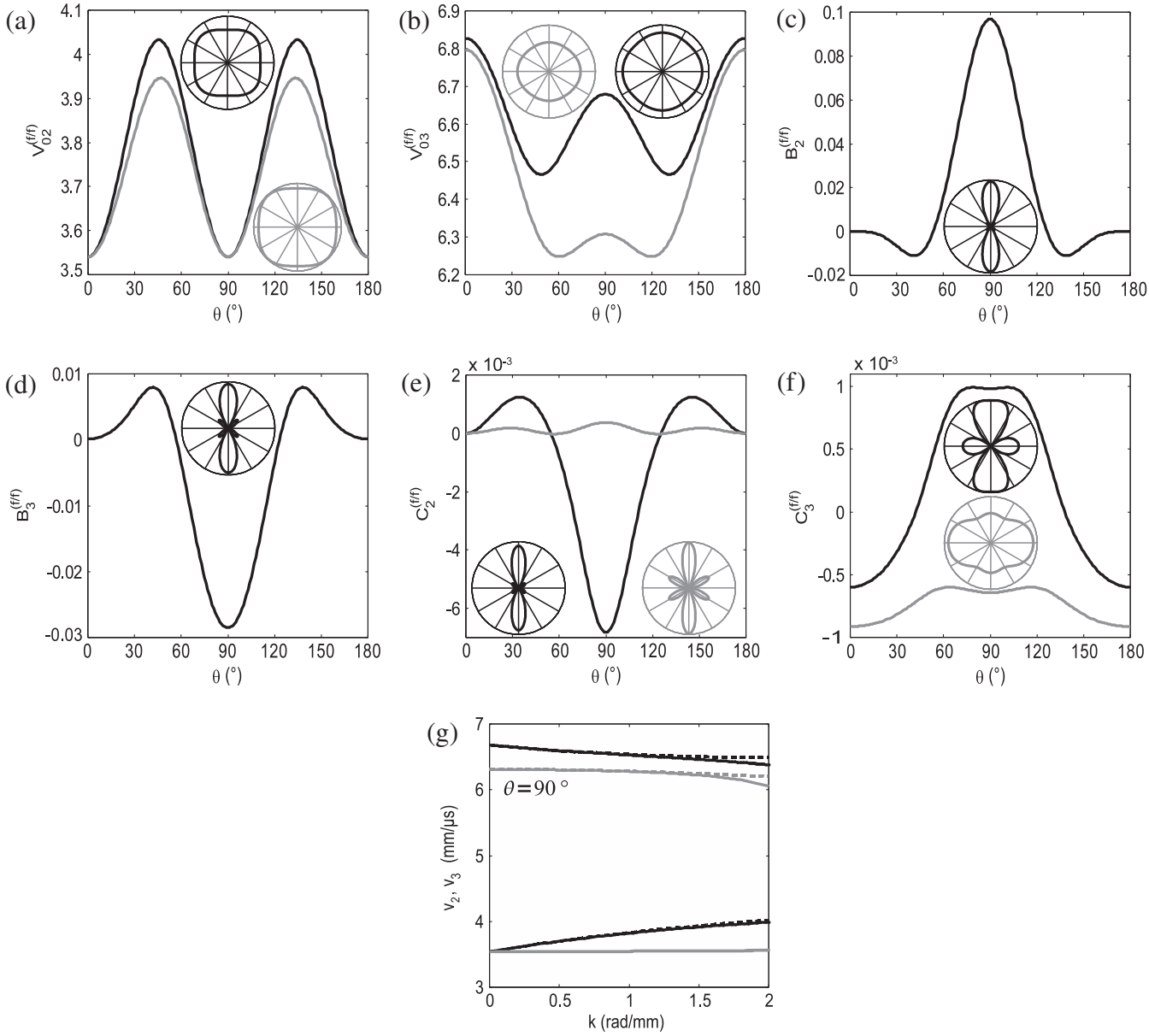

Fig. 5. The same as in Fig. 4 for the non-metallized X_2-cut $LiNbO_3$ plate (the angle θ is counted from $X_3\|3$).

$$\bar{\eta}_3 \geqslant \bar{\mu}_3 \geqslant \bar{\eta}_3^{(\mathrm{els})} \geqslant \bar{\eta}_2 \geqslant \bar{\mu}_2 \geqslant \bar{\eta}_2^{(\mathrm{els})} > 0. \tag{38}$$

Indeed, $\bar{\eta}_3 \geqslant \bar{\eta}_3^{(\mathrm{els})} \geqslant \bar{\eta}_2 \geqslant \bar{\eta}_2^{(\mathrm{els})}$ and $\bar{\eta}_3 \geqslant \bar{\mu}_3 \geqslant \bar{\eta}_2 \geqslant \bar{\mu}_2$ by the definitions of $\langle\tilde{\mathbf{n}}_3\rangle$ through $\langle\mathbf{N}_3^{(\mathrm{els})}\rangle$ and $\langle\tilde{\mathbf{n}}_3\rangle$. At the same time, $\langle\tilde{\mathbf{n}}_3\rangle - \langle\mathbf{N}_3^{(\mathrm{els})}\rangle = \langle\frac{1}{b_2}\mathbf{a}_1'\otimes\mathbf{a}_1'\rangle - \frac{1}{\langle b_2\rangle}\langle\mathbf{a}_1'\rangle\otimes\langle\mathbf{a}_1'\rangle$ is positive semi-definite by virtue of the Cauchy–Schwarz inequality, and therefore $\bar{\mu}_3 \geqslant \bar{\eta}_3^{(\mathrm{els})}$, $\bar{\mu}_2 \geqslant \bar{\eta}_2^{(\mathrm{els})}$. Combining the above inequalities yields (38).

The eigenvalues of averaged matrices are certainly not equal to the averaged eigenvalues of the varying matrices, unless the corresponding eigenvectors are independent of y. This occurs due to the appropriate symmetry rendering the eigenvectors pure longitudinal and transverse, i.e. parallel to $\mathbf{m}$ and $\mathbf{t} = \mathbf{n}\times\mathbf{m}$, whence

$$\begin{aligned}
&\bar{\eta}_T^{(\mathrm{els})} = \left\langle\eta_T^{(\mathrm{els})}\right\rangle = \left\langle\mathbf{t}\cdot\mathbf{N}_3^{(\mathrm{els})}\mathbf{t}\right\rangle,\ \bar{\eta}_L^{(\mathrm{els})} = \langle\eta_L^{(\mathrm{els})}\rangle = \left\langle\mathbf{m}\cdot\mathbf{N}_3^{(\mathrm{els})}\mathbf{m}\right\rangle;\\
&\bar{\eta}_T = \langle\eta_T\rangle = \langle\eta_T^{(\mathrm{els})}\rangle + \left\langle\frac{1}{b_2}(\mathbf{a}_1'\cdot\mathbf{t})^2\right\rangle,\ \bar{\eta}_L = \langle\eta_L\rangle = \left\langle\eta_L^{(\mathrm{els})}\right\rangle + \left\langle\frac{1}{b_2}(\mathbf{a}_1'\cdot\mathbf{m})^2\right\rangle;\\
&\bar{\mu}_T = \langle\mu_T\rangle = \langle\eta_T\rangle - \frac{1}{\langle b_2\rangle}\langle\mathbf{a}_1'\cdot\mathbf{t}\rangle^2,\ \bar{\mu}_L = \langle\mu_L\rangle = \langle\eta_L\rangle - \frac{1}{\langle b_2\rangle}\langle\mathbf{a}_1'\cdot\mathbf{m}\rangle^2,
\end{aligned} \tag{39}$$

where we follow (26) in using $\alpha = T, L$ instead of $\alpha = 2, 3$. Note that the vector $\mathbf{a}_1'(y)$ in such symmetric cases is either zero or has a constant orientation parallel to $\mathbf{m}$ or to $\mathbf{t} = \mathbf{n}\times\mathbf{m}$, see Table in Appendix.

4.2. Onset of the flexural branch

Unlike the case of a homogeneous plate, the onset slope (13) of the flexural branch $v_1(k)$ in a FG plate becomes sensitive to the type of EBC applied at its faces. Specifically, the coefficient $\kappa^{(\mathrm{f/f})} = \kappa^{(\mathrm{f/f})}$ for a FG plate with non-metallized or one-side metallized faces becomes different from $\kappa^{(\mathrm{m/m})}$ for the same plate with shorted-circuited faces. The corresponding values are given by

$$\begin{aligned}
\langle\rho\rangle\kappa^{(\mathrm{f/f})^2} &= \sum_{\alpha=2,3}\frac{1}{\bar{\eta}_\alpha}\left[\langle\widehat{F}_\alpha(\varsigma)\rangle\int_0^1\varsigma^2\widehat{F}_\alpha(\varsigma)\mathrm{d}\varsigma - \left(\int_0^1\varsigma\widehat{F}_\alpha(\varsigma)\mathrm{d}\varsigma\right)^2\right]\\
&= \sum_{\alpha=2,3}\frac{1}{\bar{\eta}_\alpha}\left[\int_0^1\int_0^\varsigma(\varsigma-\varsigma_1)^2\widehat{F}_\alpha(\varsigma)\widehat{F}_\alpha(\varsigma_1)\mathrm{d}\varsigma\mathrm{d}\varsigma_1\right],
\end{aligned} \tag{40}$$

where $\widehat{F}_\alpha(y) \equiv \mathbf{m}\cdot\hat{\mathbf{n}}_3(y)\bar{\mathbf{f}}_\alpha$, and

$$\langle\rho\rangle\kappa^{(\mathrm{m/m})^2} = \sum_{\alpha=2,3}\frac{1}{\bar{\mu}_\alpha}\left[\left\langle\widetilde{F}_\alpha(\varsigma)\right\rangle\int_0^1\varsigma^2\widetilde{F}_\alpha(\varsigma)\mathrm{d}\varsigma-\left(\int_0^1\varsigma\widetilde{F}_\alpha(\varsigma)\mathrm{d}\varsigma\right)^2\right] + \frac{1}{\langle b_2\rangle}\left[\langle\mathbf{a}_1'(\varsigma)\cdot\mathbf{m}\rangle\left(\int_0^1\varsigma^2\mathbf{a}_1'(\varsigma)\cdot\mathbf{m}\mathrm{d}\varsigma\right)-\left(\int_0^1\varsigma\mathbf{a}_1'(\varsigma)\cdot\mathbf{m}\mathrm{d}\varsigma\right)^2\right] = \int_0^1\int_0^\varsigma(\varsigma-\varsigma_1)^2\left[\sum_{\alpha=2,3}\frac{1}{\bar{\mu}_\alpha}\widetilde{F}_\alpha(\varsigma)\widetilde{F}_\alpha(\varsigma_1)+\frac{(\mathbf{a}_1'(\varsigma)\cdot\mathbf{m})(\mathbf{a}_1'(\varsigma_1)\cdot\mathbf{m})}{\langle b_2\rangle}\right]\mathrm{d}\varsigma\mathrm{d}\varsigma_1, \tag{41}$$

where $\widetilde{F}_\alpha(y)=\mathbf{m}\cdot\tilde{\mathbf{n}}_3(y)\bar{\mathbf{g}}_\alpha$. For instance, if $\mathbf{a}_1'(y)\cdot\mathbf{m}$ is an odd function w.r.t. the plate midplane, then $\widetilde{F}_\alpha(y)=\bar{F}_\alpha(y)$ and so

$$\kappa^{(\mathrm{m/m})^2}=\kappa^{(\mathrm{f/f})^2}-\frac{1}{\langle\rho\rangle\langle b_2\rangle}\left(\int_0^1\varsigma\mathbf{a}_1'(\varsigma)\cdot\mathbf{m}\mathrm{d}\varsigma\right)^2. \tag{42}$$

Without regard for piezoeffect $\left(\mathbf{a}_1'=\mathbf{0}\Rightarrow\hat{\mathbf{n}}_3,\tilde{\mathbf{n}}_3=\mathbf{N}_3^{(\mathrm{els})}\right)$, Eqs. (40) and (41) reduce to the known expression for the 'purely elastic' $\kappa^{(\mathrm{els})}$. Similarly to homogeneous plates, the flexural-branch slope in FG plates is not piezoactive, $\kappa^{(\mathrm{f/f})}=\kappa^{(\mathrm{m/\ m})}=\kappa^{(\mathrm{els})}$, when $\mathbf{a}_1'\cdot\mathbf{m}=0$ (see Table). In general,

$$\kappa^{(\mathrm{f/f})}\left(=\kappa^{(\mathrm{f/m})}\right)\geqslant\kappa^{(\mathrm{m/m})}$$

for any fixed $\mathbf{n}$ and $\mathbf{m}$ according to the formal proof of the 'slowing' effect of the metallization (Shuvalov et al., 2008). At the same time, it is not evident that the coefficient κ for an arbitrary FG piezoplate is always bounded from below by $\kappa^{(\mathrm{els})}$, as it is the case for homogeneous plates.

For the symmetric cases rendering the eigenvectors of $\mathbf{N}_3^{(\mathrm{els})}$, $\hat{\mathbf{n}}_3$, $\tilde{\mathbf{n}}_3$ parallel to $\mathbf{m}$ and $\mathbf{t}=\mathbf{n}\times\mathbf{m}$, Eqs. (40), (41) simplify in view of (39) to

$$\kappa^{(\mathrm{f/f})2}=\frac{1}{\langle\rho\rangle\langle\eta_L\rangle}\int_0^1\int_0^\varsigma(\varsigma-\varsigma_1)^2\eta_L(\varsigma)\eta_L(\varsigma_1)\mathrm{d}\varsigma\mathrm{d}\varsigma_1,$$
$$\kappa^{(\mathrm{m/m})2}=\kappa^{(\mathrm{f/f})2}-\frac{1}{\langle\rho\rangle\langle\mu_L\rangle\langle\eta_L\rangle\langle b_2\rangle}\left[\int_0^1\int_0^1(\varsigma-\varsigma_1)\eta_L(\varsigma)(\mathbf{a}_1'(\varsigma_1)\cdot\mathbf{m})\mathrm{d}\varsigma\mathrm{d}\varsigma_1\right]^2, \tag{43}$$

where $\eta_L(y)=\eta_L^{(\mathrm{els})}+(\mathbf{a}_1'\cdot\mathbf{m})^2/b_2$. In particular, Eq. (43) holds for transversely isotropic values $\kappa^{(\mathrm{f/f})}$ and $\kappa^{(\mathrm{m/m})}$ in any propagation direction $\mathbf{m}$ in the plate with the normal $\mathbf{n}$ along the threefold axis 3. Fig. 6 shows the long-wave onset of the flexural branch $v_1(k)$ computed for the non-metallized and metallized X_3-cut FG plate of $3m$ symmetry, whose material is modelled by multiplying the set of constants ρ, c_{ijkl}, e_{ijk}, ε_{ij} of PMN–33%PT (Zhang et al., 2003)

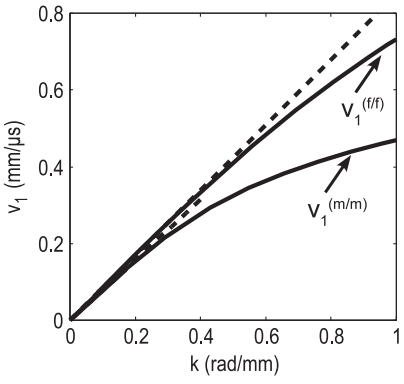

Fig. 6. The flexural-branch onset for $\mathbf{m}\|X_1$ in the X_3-cut FG plate of $3m$ symmetry with non-metallized faces $\left(v_1^{(\mathrm{f/f})}\right)$ and with short-circuited faces $\left(v_1^{(\mathrm{m/m})}\right)$. Dashed lines show the slopes $\kappa^{(\mathrm{f/f})}$ and $\kappa^{(\mathrm{m/m})}$ given by (43).

by the factor $[1+9(1-y/d)^2]$. The observed slopes $\kappa^{(\mathrm{f/f})}\approx 0.850>\kappa^{(\mathrm{m/m})}\approx 0.788(>\kappa^{(\mathrm{els})}\approx 0.697)$ verify (43) with $\eta_L(y)$ defined through the given FG material parameters according to (39), see also Section A.1 of Appendix.

In conclusion, it is noted that the displacement vector $\mathbf{A}_1(y)$ of the flexural wave taken to the first kd-order in a FG plate is, contrary to the case of a homogeneous plate, neither always non-piezoactive, nor always confined to the sagittal plane $\{\mathbf{n},\mathbf{m}\}$. For a non-metallized FG piezoplate, this vector is

$$\mathbf{A}_1^{(\mathrm{f/f})}(y)=\mathbf{n}-\mathrm{i}ky\mathbf{m}+\mathrm{i}kd\sum_{\alpha=2,3}\frac{\bar{\mathbf{f}}_\alpha}{\bar{\eta}_\alpha}\int_0^1\varsigma\widehat{F}_\alpha(\varsigma)\mathrm{d}\varsigma, \tag{44}$$

where the last term is generally piezoactive and may provide the anti-plane component $\mathbf{A}_1^{(\mathrm{f/f})}\cdot\mathbf{t}=O(kd)$ (even if the plate is purely elastic). For a homogeneous plate, (44) reduces indeed to (18).

4.3. Origin points of the upper fundamental branches

Dealing with the two upper fundamental branches in a FG piezoplate, we confine to their origin points at ω, $k\to 0$. The zero-order velocity and polarization are defined by the eigenvalues and eigenvectors (37) (see also (39)) of either $\langle\hat{\mathbf{n}}_3\rangle$ if the plate is non-metallized or one-side metallized, or of the averaged matrix $\langle\tilde{\mathbf{n}}_3\rangle$ if the plate is short-circuited, namely,

$$v_{0\alpha}^{(\mathrm{f/f})}=v_{0\alpha}^{(\mathrm{f/m})}=\sqrt{\bar{\eta}_\alpha/\langle\rho\rangle},\ v_{0\alpha}^{(\mathrm{m/m})}=\sqrt{\bar{\mu}_\alpha/\langle\rho\rangle};\quad \mathbf{A}_{0\alpha}^{(\mathrm{f/f})}=\mathbf{A}_{0\alpha}^{(\mathrm{f/m})}=\bar{\mathbf{f}}_\alpha,\ \mathbf{A}_{0\alpha}^{(\mathrm{m/m})}=\bar{\mathbf{g}}_\alpha,\quad \alpha=2,3, \tag{45}$$

whereas $v_{0\alpha}^{(\mathrm{els})}=\sqrt{\bar{\eta}_\alpha^{(\mathrm{els})}/\langle\rho\rangle}$ and $\mathbf{A}_{0\alpha}^{(\mathrm{els})}=\bar{\mathbf{f}}_\alpha^{(\mathrm{els})}$ for purely elastic FG plates. It is seen that the values $v_{0\alpha}^{(\mathrm{m/m})}$ for a FG short-circuited plate become generally piezoactive, unlike the case of homogeneous plates where $v_{0\alpha}^{(\mathrm{m/m})}=v_{0\alpha}^{(\mathrm{els})}$ (see (20)). By virtue of (38), the general hierarchy of the zero-order velocity values in any FG piezoplate is

$$v_{03}^{(\mathrm{f/f})}=v_{03}^{(\mathrm{f/m})}\geqslant v_{03}^{(\mathrm{m/m})}\geqslant v_{03}^{(\mathrm{els})} \geqslant v_{02}^{(\mathrm{f/f})}=v_{02}^{(\mathrm{f/m})}\geqslant v_{02}^{(\mathrm{m/m})}\geqslant v_{02}^{(\mathrm{els})}. \tag{46}$$

If $\mathbf{a}_1'(y)\cdot\mathbf{m}$ is an odd function w.r.t. the plate midplane, then the definition (36) implies $\hat{\mathbf{n}}_3=\tilde{\mathbf{n}}_3(\neq\mathbf{N}_3^{(\mathrm{els})})$ and so $v_{0\alpha}^{(\mathrm{f/f})}=v_{0\alpha}^{(\mathrm{m/m})}\geqslant v_{0\alpha}^{(\mathrm{els})}$.

If $\mathbf{a}_1'\cdot\mathbf{m}=0$ then all three matrices $\hat{\mathbf{n}}_3$, $\tilde{\mathbf{n}}_3$, $\mathbf{N}_3^{(\mathrm{els})}$ coincide. Hence the zero-order velocity $v_{0\alpha}$ in FG plates is non-piezoactive for the same symmetric orientations as for homogeneous plates, see Table. Also the isotropy (azimuthal invariance) of the limit ω, $k\to 0$ in a plate with the normal $\mathbf{n}\|3$ remains valid for FG plates. In this case, except for the 32 class, the zero-order longitudinal wave velocity v_{0L} is piezoactive, now for both non-metallized and short-circuited plates: for example, Eqs. (39) and (45) yield $v_{0L}^{(\mathrm{f/f})}=3.452$, $v_{0L}^{(\mathrm{m/m})}=3.094$, $v_{0L}^{(\mathrm{els})}=2.830$ mm/μs for any $\mathbf{m}$ in the X_3-cut FG plate exemplified in Fig. 6. Note that the discrepancy between the above values of $v_{0L}^{(\mathrm{m/m})}$ and $v_{0L}^{(\mathrm{els})}$ is an indicator of the material heterogeneity.

5. Conclusions

Impact of piezoelectricity on the low-frequency long-wave onset of the fundamental plate branches at $kd\ll 1$ can raise the slope κ of the flexural branch $v_1(k)$, increase the zero-order velocity $v_{0\alpha}$ at ω, $k\to 0$ for the two upper branches $v_\alpha(k)$ ($\alpha=2,3$) and induce their linear dispersion. The latter feature is especially significant because it is ruled out 'by the first principles' in purely elastic plates; therefore it is of itself an instantaneous indicator that the plate material is piezoelectric. The low-frequency effect of piezoelectricity depends on the plate-wave geometry and, in certain cases, on the type of electric boundary conditions (EBC) supplied at the plate faces. For instance, the flexural-branch slope and the ω, $k\to 0$ limit of the upper branches $v_\alpha(k)$ are non-piezoactive in

a plate parallel to the symmetry plane, and so are the zero- and first-order parameters of these branches in a short-circuited homogeneous piezoplate.

The paper presents a detailed analysis of the problem for arbitrary anisotropy and various types of the EBC. Explicit expressions for the onset of the fundamental branches are obtained, and their azimuthal variation is exemplified for different plate orientations. Certain invariant inequalities between the long-wave parameters for a plate under different EBC are established. The flexural-branch slope κ and the zero-order velocity $v_{0\alpha}$ are also derived for the functionally graded (FG) plates. It is noted that the FG plates are more sensitive to the type of EBC: in contrast to any homogeneous plate, the slope κ for a non-metallized plate becomes generally different from κ for this plate being short-circuited and the velocity $v_{0\alpha}$ in a short-circuited plate becomes generally piezoactive entirely due to the material heterogeneity. At the same time, the plate-wave geometrical settings, for which κ and $v_{0\alpha}$ are non-piezoactive under any EBC, remain intact, i.e. are the same for both homogeneous and FG plates, see Table. Note also that κ and $v_{0\alpha}$ are azimuthally invariant in the X_3-cut trigonal or $\langle 111\rangle$-cut cubic homogeneous and FG plates.

Appendix A

A.1. Background parameters for $\mathbf{n}\|3$

Let $\mathbf{n}$ be fixed along the threefold axis 3 of a trigonal or cubic piezoelectric medium. Choose the crystallographic basis with $X_3\|3$ as the reference for the components of material tensors and take

$$\mathbf{m}=(\cos\theta,\sin\theta,0)^{\mathrm{T}},\quad \mathbf{t}\equiv\mathbf{n}\times\mathbf{m}=(-\sin\theta,\cos\theta,0)^{\mathrm{T}}. \tag{47}$$

Consider the background parameters introduced in (4), (5). Interestingly, the Stroh-matrix block $\mathbf{N}_3^{(\mathrm{els})}$ for the case in hand is transversely isotropic:

$$\begin{aligned}&\mathbf{N}_3^{(\mathrm{els})}=\eta_L^{(\mathrm{els})}\mathbf{m}\otimes\mathbf{m}+\eta_T^{(\mathrm{els})}\mathbf{t}\otimes\mathbf{t}\\ &\text{with }\eta_L^{(\mathrm{els})}=c_{11}-\frac{c_{13}^2}{c_{33}}-\frac{c_{14}^2+c_{25}^2}{c_{44}},\ \eta_T^{(\mathrm{els})}=c_{66}-\frac{c_{14}^2+c_{25}^2}{c_{44}}.\end{aligned} \tag{48}$$

The vectors $\mathbf{a}$ and scalars b specify as

$$\begin{aligned}&\mathbf{a}_1=-\frac{1}{c_{44}}(e_{15}\mathbf{m}+e_{14}\mathbf{t}),\ \mathbf{a}_1'=\frac{e_{31}c_{33}-e_{33}c_{13}}{\varepsilon_{33}c_{33}+e_{33}^2}\mathbf{m},\ \mathbf{a}_2=-\frac{e_{33}}{\varepsilon_{33}c_{33}+e_{33}^2}\mathbf{n},\\ &\mathbf{a}_3=\left(e_{11}+\frac{e_{15}c_{25}}{c_{44}}-\frac{e_{14}c_{14}}{c_{44}}\right)\begin{pmatrix}\cos2\theta\\-\sin2\theta\\0\end{pmatrix}-\left(e_{22}+\frac{e_{15}c_{14}}{c_{44}}+\frac{e_{14}c_{25}}{c_{44}}\right)\begin{pmatrix}\sin2\theta\\\cos2\theta\\0\end{pmatrix};\\ &b_1=0,\ b_2=\frac{1}{\varepsilon_{33}+e_{33}^2/c_{33}},\ b_3=-\varepsilon_{11}-\frac{e_{14}^2+e_{15}^2}{c_{44}},\end{aligned} \tag{49}$$

where certain coefficients vanish for the higher-symmetry piezoelectric classes. In particular, $\mathbf{a}_1'=\mathbf{0}$ for the 32 symmetry class due to $e_{31}=e_{33}=0$. In turn, Eqs. (48), (49) with $c_{25}=0$, $e_{11}=e_{14}=0$ correspond to the $3m$ and 23, $\bar{4}3m$ classes, with a standard use of 'rotated' constants in $X_3\|3\|\langle 111\rangle$ for the cubic case.

By virtue of $\mathbf{a}_1'\|\mathbf{m}$ (unless it is zero for 32), the matrix $\hat{\mathbf{n}}_3=\mathbf{N}_3^{(\mathrm{els})}+\frac{1}{b_2}\mathbf{a}_1'\otimes\mathbf{a}_1'$ is also transversely isotropic likewise $\mathbf{N}_3^{(\mathrm{els})}$. As a result, the leading-order dispersion coefficient κ at the flexural-branch onset and the limit $\omega, k\to 0$ for the two upper fundamental branches are transversely isotropic in any homogeneous or FG plate which is cut orthogonally to the threefold axis 3, see Sections 3, 4.

A.2. Background parameters for $\mathbf{n}\perp m$ and $\mathbf{n}\|2$

Suppose that $\mathbf{n}$ is orthogonal to the symmetry plane m in a monoclinic medium. Assume the reference basis with $X_1\|\mathbf{n}$ and take

$$\mathbf{m}=(0,\sin\theta,\cos\theta)^{\mathrm{T}},\quad \mathbf{t}\equiv\mathbf{n}\times\mathbf{m}=(0,-\cos\theta,\sin\theta)^{\mathrm{T}}. \tag{50}$$

Explicit form of the Stroh matrix $\mathbf{N}^{(\mathrm{els})}$ for $\mathbf{m}$ varying in m may be found in Shuvalov (2000). In particular

$$\begin{aligned}&\mathbf{N}_3^{(\mathrm{els})}=\begin{pmatrix}0&0&0\\0&C\cos^2\theta+E\sin2\theta+F\sin^2\theta&B\cos^2\theta+\frac{1}{2}D\sin2\theta+E\sin^2\theta\\0&B\cos^2\theta+\frac{1}{2}D\sin2\theta+E\sin^2\theta&A\cos^2\theta+B\sin2\theta+C\sin^2\theta\end{pmatrix},\\ &\text{where}\quad A=c_{33}-\tfrac{c_{13}^2}{c_{11}},\ B=c_{34}-\tfrac{c_{13}c_{14}}{c_{11}},\ C=c_{44}-\tfrac{c_{14}^2}{c_{11}},\\ &\qquad D=c_{23}+c_{44}-\tfrac{c_{12}c_{13}+c_{14}^2}{c_{11}},\ E=c_{24}-\tfrac{c_{12}c_{14}}{c_{11}},\ F=c_{22}-\tfrac{c_{12}^2}{c_{11}}.\end{aligned} \tag{51}$$

The (non-zero) eigenvalues $\eta_{2,3}^{(\mathrm{els})}$ and the corresponding eigenvectors $\mathbf{f}_{2,3}^{(\mathrm{els})}$ of $\mathbf{N}_3^{(\mathrm{els})}$ define the zero-order velocity (31). The vectors $\mathbf{a}$ and scalars b specify as follows:

$$\begin{aligned}&b_1=0,\ b_2=\left(\varepsilon_{33}+\frac{c_{55}e_{16}^2-2c_{56}e_{15}e_{16}+c_{66}e_{15}^2}{c_{55}c_{66}-c_{56}^2}\right)^{-1},\ b_3=\varepsilon_{11}-\frac{(e_{31}\cos\theta+e_{21}\sin\theta)^2}{c_{11}};\\ &\mathbf{a}_1'=\mathbf{0};\ \mathbf{a}_1=-\frac{1}{c_{11}}(e_{31}\cos\theta+e_{21}\sin\theta)\mathbf{n};\ \mathbf{a}_2=-\frac{b_2}{c_{55}c_{66}-c_{56}^2}\begin{pmatrix}0\\c_{55}e_{16}-c_{56}e_{15}\\-c_{56}e_{16}+c_{66}e_{15}\end{pmatrix},\\ &\mathbf{a}_3=\begin{pmatrix}0\\\left(e_{34}-\frac{c_{14}e_{31}}{c_{11}}\right)\cos^2\theta+\frac{1}{2}\left(e_{24}+e_{32}-\frac{c_{14}e_{21}}{c_{11}}-\frac{c_{12}e_{31}}{c_{11}}\right)\sin2\theta+\left(e_{22}-\frac{c_{12}e_{21}}{c_{11}}\right)\sin^2\theta\\\left(e_{33}-\frac{c_{13}e_{31}}{c_{11}}\right)\cos^2\theta+\frac{1}{2}\left(e_{23}+e_{34}-\frac{c_{13}e_{21}}{c_{11}}-\frac{c_{14}e_{31}}{c_{11}}\right)\sin2\theta+\left(e_{24}-\frac{c_{14}e_{21}}{c_{11}}\right)\sin^2\theta\end{pmatrix}.\end{aligned} \tag{52}$$

Next let $\mathbf{n}$ be parallel to the twofold axis 2 in a monoclinic medium. This case is equivalent to the above case $\mathbf{n}\perp m$ within the framework of pure elasticity, but is different from it with regard for the piezoeffect. Keeping the basis $X_1\|\mathbf{n}(\|2)$ and the azimuth angle θ as in (50), it now follows that

$$\begin{aligned}&b_1=0,\quad b_2=\frac{1}{\varepsilon_{11}+e_{11}^2/c_{11}},\\ &\mathbf{a}_1'=b_2\begin{pmatrix}0\\\left(e_{14}-e_{11}\frac{c_{14}}{c_{11}}\right)\cos\theta+\left(e_{12}-e_{11}\frac{c_{12}}{c_{11}}\right)\sin\theta\\\left(e_{13}-e_{11}\frac{c_{13}}{c_{11}}\right)\cos\theta+\left(e_{14}-e_{11}\frac{c_{14}}{c_{11}}\right)\sin\theta\end{pmatrix},\\ &\mathbf{a}_2=-b_2\frac{e_{11}}{c_{11}}\mathbf{n},\ \mathbf{a}_3=\mathbf{0},\end{aligned} \tag{53}$$

where lengthy expressions for b_3 and $\mathbf{a}_1(\perp\mathbf{n})$ are omitted.

A.3. Overview of the symmetric cases

The benchmarks of the auxiliary vectors $\mathbf{a}_1',\mathbf{a}_3$ and of the eigenvectors $\mathbf{f}_\alpha^{(\mathrm{els})}$, $\mathbf{f}_\alpha$ and eigenvalues $\eta_\alpha^{(\mathrm{els})}$, η_α of the matrices $\mathbf{N}_3^{(\mathrm{els})}$ and $\hat{\mathbf{n}}_3$ are recapped in Table (where $\alpha=2,3\Rightarrow\alpha=T,L$ when $\mathbf{f}_\alpha^{(\mathrm{els})}$, $\mathbf{f}_\alpha$ coincide with $\mathbf{t}\equiv\mathbf{n}\times\mathbf{m}$ and $\mathbf{m}$) (See Table 1). According to (14), (20) and (21), this data provides quick basic insight into the zero- and first-order parameters at the onset of the fundamental branches in a homogeneous piezoelectric plate under different types of EBC at its faces. Moreover, the non-piezoactive cases $\kappa=\kappa^{(\mathrm{els})}, v_{0\alpha}=v_{0\alpha}^{(\mathrm{els})}$ pointed out in Table qualify as such for FG plates as well.

It is noted that the strong-inequality signs in the upper rows of Table correspond to an arbitrary, generic orientation of the propagation direction $\mathbf{m}$ (indicated as '$\forall\mathbf{m}$') in the fixed plane with a given normal $\mathbf{n}$. The settings which assume a fixed symmetric orientation of $\mathbf{m}$ in this plane are considered in the four lower rows. The properties of vectors $\mathbf{a}_1',\mathbf{a}_3$ certainly follow the

Table 1
Benchmarks of the auxiliary vectors $\mathbf{a}_1'$, $\mathbf{a}_3$; the slope κ (14) of the flexural branch $v_1(k)$; the zero-order polarization $\mathbf{A}_{0\alpha}$ and velocity $v_{0\alpha}$ (20) of the upper fundamental branches $v_\alpha(k)$, $\alpha = 2, 3$, and their linear-dispersion coefficients B_α (21) in a homogeneous piezoplate.

Orientation	$\mathbf{a}_1'$	$\mathbf{a}_3$	κ, $\kappa^{(\mathrm{els})}$	$\mathbf{A}_{0\alpha}^{(\mathrm{f/f})}$, $\mathbf{A}_{0\alpha}^{(\mathrm{els})}$	$v_{0\alpha}^{(\mathrm{f/f})}$, $v_{0\alpha}^{(\mathrm{els})}$	$B_\alpha^{(\mathrm{f/f})}$	$B_\alpha^{(\mathrm{f/m})}$
$\mathbf{n}\perp m$, $\forall\mathbf{m}$	$\mathbf{0}$	$\nparallel \mathbf{m},\mathbf{t}$	=	= , $\nparallel \mathbf{m},\mathbf{t}$	=	>0	0
$\mathbf{n}\parallel 2, \bar{4}$, $\forall\mathbf{m}$	$\nparallel \mathbf{m},\mathbf{t}$	$\mathbf{0}$	>	$\neq$, $\nparallel \mathbf{m},\mathbf{t}$	>	<0	$2B_\alpha^{(\mathrm{f/f})}$
$\mathbf{n}\parallel 3$, $\forall\mathbf{m}$ $G \neq 32$	$\parallel\mathbf{m}$	$\nparallel \mathbf{m},\mathbf{t}$	>	$\mathbf{A}_{0T}=\mathbf{t}$ $\mathbf{A}_{0L}=\mathbf{m}$	= >	>0 $\lesseqgtr 0$	0 <0
$\mathbf{n}\parallel 3$, $\forall\mathbf{m}$ $G = 32$	$\mathbf{0}$	$\nparallel \mathbf{m},\mathbf{t}$	=	$\mathbf{A}_{0T}=\mathbf{t}$ $\mathbf{A}_{0L}=\mathbf{m}$	=	>0	0
$\mathbf{n}\parallel \bar{6}$, $\forall\mathbf{m}$	$\mathbf{0}$	$\nparallel \mathbf{m},\mathbf{t}$	=	$\mathbf{A}_{0T}=\mathbf{t}$ $\mathbf{A}_{0L}=\mathbf{m}$	=	>0	0
$\mathbf{n}\parallel 4$, $\forall\mathbf{m}$ $G \neq 422$	$\parallel\mathbf{m}$	$\mathbf{0}$	>	= , $\nparallel \mathbf{m},\mathbf{t}$	>	<0	$2B_\alpha^{(\mathrm{f/f})}$
$\mathbf{n}\parallel 6$, $\forall\mathbf{m}$ $G \neq 622$	$\parallel\mathbf{m}$	$\mathbf{0}$	>	$\mathbf{A}_{0T}=\mathbf{t}$ $\mathbf{A}_{0L}=\mathbf{m}$	= >	0 <0	0 $2B_\alpha^{(\mathrm{f/f})}$
$\mathbf{n}\parallel 4$, $G = 422$ $\mathbf{n}\parallel 6$, $G = 622$	$\mathbf{0}$	$\mathbf{0}$	=	= , $\nparallel \mathbf{m},\mathbf{t}$ $\mathbf{A}_{0T,0L}=\mathbf{m},\mathbf{t}$	=	0	0
$\mathbf{n}\perp 2$, $\mathbf{m}\parallel 2$	$\parallel\mathbf{t}$	$\parallel\mathbf{m}$	=	$\mathbf{A}_{0T}=\mathbf{t}$ $\mathbf{A}_{0L}=\mathbf{m}$	> =	<0 >0	$2B_\alpha^{(\mathrm{f/f})}$ 0
$\mathbf{n}\perp 2$, $\mathbf{t}\parallel 2$	$\parallel\mathbf{t}$	$\parallel\mathbf{t}$	=	$\mathbf{A}_{0T}=\mathbf{t}$ $\mathbf{A}_{0L}=\mathbf{m}$	> =	$\lesseqgtr 0$ 0	<0 0
$\mathbf{n}\parallel m$, $\mathbf{m}\perp m$	$\parallel\mathbf{m}$	$\parallel\mathbf{t}$	>	$\mathbf{A}_{0T}=\mathbf{t}$ $\mathbf{A}_{0L}=\mathbf{m}$	= >	>0 <0	0 $2B_\alpha^{(\mathrm{f/f})}$
$\mathbf{n}\parallel m$, $\mathbf{t}\perp m$	$\parallel\mathbf{m}$	$\parallel\mathbf{m}$	>	$\mathbf{A}_{0T}=\mathbf{t}$ $\mathbf{A}_{0L}=\mathbf{m}$	= >	uncoupled SH_0 $\lesseqgtr 0$	 <0

symmetry subordination implying that, e.g., a conjunction of the cases $\mathbf{n}\perp m$ and $\mathbf{n}\parallel 3$ yields the results for $\mathbf{n}\parallel\bar{6}$, same for $\mathbf{n}\parallel 3$ and $\mathbf{n}\parallel 2$ leads to $\mathbf{n}\parallel 6$, etc. Some other high-symmetry cases not mentioned in Table are similarly evident on these grounds.

A.4. Wave-field dispersion at the onset of upper fundamental branches

The leading-order dispersion of the amplitudes of elastic displacement, potential and electric displacement associated with two upper fundamental branches $v_{2,3}(k)$ in a non-metallized plate $y\in[0,d]$ is

$$\begin{aligned}
\mathbf{A}_\alpha^{(\mathrm{f/f})}(y) &= \mathbf{A}_{0\alpha}^{(\mathrm{f/f})} + \mathrm{i}k\Big(y-\frac{d}{2}\Big)\hat{\mathbf{n}}_1\mathbf{f}_\alpha + \mathrm{i}k\frac{d}{2}\mathbf{f}_\alpha(\mathbf{f}_\alpha\cdot\hat{\mathbf{n}}_1\mathbf{f}_\alpha)\\
&\quad + k\frac{d}{2}\mathbf{f}_\beta\frac{\varepsilon_0^{-1}(\mathbf{a}_3\cdot\mathbf{f}_\alpha)(\mathbf{a}_3\cdot\mathbf{f}_\beta)-\varepsilon_0(\mathbf{a}_1'\cdot\mathbf{f}_\alpha)(\mathbf{a}_1'\cdot\mathbf{f}_\beta)}{\eta_\alpha-\eta_\beta}, \quad \alpha,\beta=2,3,\alpha\neq\beta;\\
\phi_\alpha^{(\mathrm{f/f})}(y) &= \mathrm{i}k\Big(y-\frac{d}{2}\Big)(\mathbf{a}_1'\cdot\mathbf{m}) + k\frac{d}{2}\frac{\mathbf{a}_3\cdot\mathbf{m}}{\varepsilon_0},\\
k^{-1}D_{y\alpha}^{(\mathrm{f/f})}(y) &= k\Big(y-\frac{d}{2}\Big)(\mathbf{a}_3\cdot\mathbf{m}) + \mathrm{i}k\frac{d}{2}\varepsilon_0(\mathbf{a}_1'\cdot\mathbf{m}),
\end{aligned} \tag{54}$$

where $\mathbf{A}_{0\alpha}^{(\mathrm{f/f})}=\mathbf{f}_\alpha$, see (20). The traction amplitude $\mathrm{i}k^{-1}\mathbf{F}_\alpha$ is, as usual, of the order $(kd)^2$. For a short-circuited plate, $\mathbf{A}_\alpha^{(\mathrm{m/m})}$ is given by (54_1) without piezoelectric terms, i.e. $\mathbf{A}_\alpha^{(\mathrm{m/m})}=\mathbf{A}_\alpha^{(\mathrm{els})}$ up to the first order in kd, and the dispersion of $\phi_\alpha^{(\mathrm{m/m})}$ starts from the $(kd)^2$-order (due to $\phi=0$ at the faces), while $\mathrm{i}k^{-1}D_{y\alpha}^{(\mathrm{m/m})}$ starts from the term $\frac{1}{b_2}\mathbf{a}_1'\cdot\mathbf{f}_\alpha^{(\mathrm{els})}$ which, when non-zero, is of the order of piezoelectric coupling.

The vectors $\hat{\mathbf{n}}_1\mathbf{f}_\alpha$ and $\mathbf{N}_1^{(\mathrm{els})}\mathbf{f}_\alpha^{(\mathrm{els})}$ $(\alpha=2,3)$ appearing in the first-order perturbation of the elastic displacement $\mathbf{A}_\alpha^{(\mathrm{f/f})}$ and $\mathbf{A}_\alpha^{(\mathrm{els})}$ may generally have any orientation with respect to the reference frame of orthogonal vectors $\mathbf{n}$ and $\mathbf{f}_{2,3}$ or $\mathbf{f}_{2,3}^{(\mathrm{els})}$. At the same time, a 'pure piezoelectric' component of this perturbation can be singled out for plates of certain symmetric cuts. For example, this is the case if the plate is parallel to the symmetry plane or orthogonal to the twofold axis, so that $\mathbf{n}\perp m$ or $\mathbf{n}\parallel 2$. Then $\hat{\mathbf{n}}_1\mathbf{f}_\alpha\parallel\mathbf{n}$ for $\alpha=2,3$ and hence Eq. (54_1) with reference to Table yields

$$\begin{aligned}
\mathbf{A}_\alpha^{(\mathrm{f/f})}(y) &= \mathbf{f}_\alpha^{(\mathrm{els})} + \mathrm{i}k\Big(y-\frac{d}{2}\Big)\mathbf{N}_1^{(\mathrm{els})}\mathbf{f}_\alpha^{(\mathrm{els})} + k\frac{d}{2}\mathbf{f}_\beta^{(\mathrm{els})}\frac{\varepsilon_0^{-1}\big(\mathbf{a}_3\cdot\mathbf{f}_\alpha^{(\mathrm{els})}\big)\big(\mathbf{a}_3\cdot\mathbf{f}_\beta^{(\mathrm{els})}\big)}{\eta_\alpha^{(\mathrm{els})}-\eta_\beta^{(\mathrm{els})}} \quad \text{for } \mathbf{n}\perp m,\\
\mathbf{A}_\alpha^{(\mathrm{f/f})}(y) &= \mathbf{f}_\alpha + \mathrm{i}ky\hat{\mathbf{n}}_1\mathbf{f}_\alpha + k\frac{d}{2}\mathbf{f}_\beta\frac{\varepsilon_0(\mathbf{a}_1'\cdot\mathbf{f}_\alpha)(\mathbf{a}_1'\cdot\mathbf{f}_\beta)}{\eta_\alpha-\eta_\beta} \quad \text{for } \mathbf{n}\parallel 2,
\end{aligned} \tag{55}$$

whereas $\mathbf{A}_\alpha^{(\mathrm{els})}(y)=\mathbf{f}_\alpha^{(\mathrm{els}k)}+\mathrm{i}k(y-\frac{d}{2})\mathbf{N}_1^{(\mathrm{els})}\mathbf{f}_\alpha^{(\mathrm{els})}$, in which $\mathbf{N}_1^{(\mathrm{els})}\mathbf{f}_\alpha^{(\mathrm{els})}$ $(=\hat{\mathbf{n}}_1\mathbf{f}_\alpha$ for $\mathbf{n}\perp m)$ is also parallel to $\mathbf{n}$. Therefore, for both plate orientations $\mathbf{n}\perp m$ and $\mathbf{n}\parallel 2$, the departure of the first-order perturbation of $\mathbf{A}_\alpha^{(\mathrm{f/f})}$ from the plane spanned by the zero-order polarization $\mathbf{A}_{0\alpha}^{(\mathrm{f/f})}$ and the plate normal $\mathbf{n}$ is entirely caused by the piezoeffect.

References

Cheng, Z.-Q., Reddy, J.N., 2003. An asymptotic theory for vibrations of inhomogeneous/laminated piezoelectric plates. IEEE Transactions on Ultrasonics, Ferroelectrics, and Frequency Control 50, 1436–1443.

Dieulesaint, E., Royer, D., 1980. Elastic Waves in Solids. John Wiley, New York.

Johansson, G., Niklasson, A.J., 2003. Approximate dynamic boundary conditions for a thin piezoelectric layer. International Journal of Solids and Structures 40, 3477–3492.

Joshi, S.G., Zaitsev, B.D., Kuznetsova, I.E., Teplykh, A.A., Pasachhe, A., 2006. Characteristics of fundamental acoustic wave modes in thin piezoelectric plates. Ultrasonics 44 (1), E787–E791.

Krommer, M., 2003. Piezoelastic vibrations of composite Reissner–Mindlin-type plates. Journal of Sound and Vibration 263, 871–891.

Kuznetsova, I.E., Zaitsev, B.D., Teplykh, A.A., Joshi, S.G., Kuznetsova, A.S., 2008. The power flow angle of acoustic waves in thin piezoelectric plates. IEEE Transactions on Ultrasonics, Ferroelectrics, and Frequency Control 55, 1984–1991.

Lothe, J., Barnett, D.M., 1976. Integral formalism for surface waves in piezoelectric crystals. Existence considerations. Journal of Applied Physics 47, 1799–1807.

Lothe, J., Barnett, D.M., 1977. Further development of the theory of surface waves in piezoelectric crystals. Physica Norvegica 8, 239–254.

Mauritsson, K., 2009. Modelling of finite piezoelectric patches: comparing an approximate power series expansion theory with exact theory. International Journal of Solids and Structures 46, 1053–1065.

Mauritsson, K., Bostrom, A., Folkow, P.D., 2008. Modelling of thin piezoelectric layers on plates. Wave Motion 45, 616–628.

Poncelet, O., Shuvalov, A.L., Kaplunov, J.D., 2006. Approximation of the flexural velocity branch in plates. International Journal of Solids and Structures 43, 6329–6346.

Shuvalov, A.L., 1999. Properties of acoustic polarization in a symmetry plane of monoclinic and higher-symmetry media. Mathematics and Mechanics of Solids 4, 499–512.

Shuvalov, A.L., 2000. On the theory of wave propagation in anisotropic plates. Proceedings of the Royal Society A 456, 2197–2222.

Shuvalov, A.L., 2004. General relationships for guided acoustic waves in anisotropic plates. Proceedings of the Royal Society A 460, 2671–2679.

Shuvalov, A.L., 2006. On the impact of anisotropy on dispersion spectra of acoustic waves in plates. Comptes Rendus Mécanique 334, 243–251.

Shuvalov, A.L., Poncelet, O., Baron, C., Deschamps, M., 2005. Long-wavelength dispersion of acoustic waves in transversely inhomogeneous anisotropic plates. Wave Motion 42, 367–382.

Shuvalov, A.L., Le Clezio, E., Feuillard, G., 2008. The state-vector formalism and the Peano-series solution for modelling guided waves in functionally graded anisotropic piezoelectric plates. International Journal of Engineering Science 46, 929–947.

Ting, T.C.T., 1996. Anisotropic Elasticity. Oxford University Press, Oxford.

Wang, L., Rokhlin, S.I., 2004. Modeling of wave propagation in layered piezoelectric media by a recursive asymptotic method. IEEE Transactions on Ultrasonics, Ferroelectrics, and Frequency Control 51, 1060–1071.

Wu, C.Y., Chang, J.S., Wu, K.C., 2005. Analysis of wave propagation in infinite piezoelectric plates. Journal of Mechanics 21, 103–108.

Yang, C.H., Chimenti, D.E., 1995. Guided plate waves in piezoelectrics immersed in a dielectric fluid. I. Analysis. II. Experiments. Journal of the Acoustical Society of America 97, 2103–2115.

Yang, C.H., Huang, M.F., 2003. Measurements and modelling for the dispersion relations of acoustic waves propagating in a free piezoelectric plate. Chinese Journal of Mechanics A 19, 311–318.

Zakharov, D.D., Becker, W., 2000. 2D problems of thin anisotropic laminates. Zeitschrift fur Angewandte Mathematik und Physik 51, 555–572.

Zhang, R., Jiang, B., Cao, W., 2003. Single-domain properties of $0.67Pb(Mg_{1/3}Nb_{2/3})O_3$-$0.33PbTiO_3$ single crystals under electric field bias. Applied Physics Letters 82, 787–789.